minerals

MDPI

Article

Opening and Spreading Processes of the Eastern Paleo-Tethys Ocean: Paleomagnetic Insights from the South China Block

Yilian Liao [1,2], Baochun Huang [1,*], Claire I. O. Nichols [2], Rong Huang [1], Qishun Sun [1], Zaixu Chen [1], Zhenyang Lai [3], Danxin Li [3], Enxiong Zhou [3], Zhiyu Yi [4] and Yonggang Yan [3]

[1] Laboratory of Orogenic Belts and Crustal Evolution, School of Earth and Space Sciences, Peking University, Beijing 100871, China; yilianliao@alumni.pku.edu.cn (Y.L.); ronghuang@pku.edu.cn (R.H.); zaixuchen@stu.pku.edu.cn (Z.C.)
[2] Department of Earth Sciences, University of Oxford, Oxford OX1 3AN, UK; claire.nichols@earth.ox.ac.uk
[3] Guangdong Provincial Key Laboratory of Geodynamics and Geohazards, School of Earth Sciences and Engineering, Sun Yat-Sen University, Zhuhai 519000, China; laizhy9@mail2.sysu.edu.cn (Z.L.); zhouenx@mail2.sysu.edu.cn (E.Z.); yanyongg@mail.sysu.edu.cn (Y.Y.)
[4] Planetary Environment and Astrobiological Research Laboratory (PEARL), School of Atmospheric Sciences, Sun Yat-Sen University, Zhuhai 519000, China; yizhy5@mail.sysu.edu.cn
* Correspondence: bchuang@pku.edu.cn

Abstract

The scarcity of high-quality Paleozoic paleomagnetic data from the South China Block (SCB) has rendered the kinematic history of its rifting and drifting from Gondwana highly debated, consequently leaving the timing of opening and subsequent spreading of the Ailaoshan-Songma eastern Paleo-Tethys Ocean (ASePTO) poorly constrained. Here we report new paleomagnetic results from Givetian (~385 Ma) limestones of Dushan County, Guizhou, yielding a characteristic remanent magnetization (ChRM-B). Although the ChRM-B predominantly shows single polarity and an inconclusive fold test, multiple lines of evidence support its primary origin: (i) the corresponding paleomagnetic pole (29.5° N, 229.8° E; $dp/dm = 2.0°/3.8°$) differs substantially from all post-Middle Devonian SCB poles; (ii) rock magnetic analyses combined with high-resolution transmission electron microscopy indicate that nanoscale detrital magnetite and maghemite are the main remanence carriers; and (iii) statistical consistency between the 7 site-mean directions of the ChRM-B and 34 coeval site-mean directions from the published Yuntaiguan Formation red bed records in western Hunan. In the light of the compatible ages and geological settings of the sampling strata from the two sampling areas, the two datasets were combined to derive a robust Middle Devonian paleomagnetic pole for the SCB. The merged dataset (41 sites) yields mean directions of $D_g/I_g = 37.2°/-18.9°$ ($k_g = 46.4$, $\alpha_{95} = 3.3°$) before, and $D_s/I_s = 43.1°/-23.8°$ ($k_s = 54.4$, $\alpha_{95} = 3.1°$) after the *tilt-correction* with a B-class reversals test and a positive fold test. The new robust paleomagnetic pole for the SCB, at 33.2° N, 234.7° E with $A_{95} = 2.4°$ and reliability index R = 7, when integrated with other reliable paleomagnetic records, allows the construction of an updated apparent polar wander path (APWP) for the SCB. Comparison with the synthetic APWP of Gondwana enables the reconstruction of the opening of the ASePTO at ~410–400 Ma, followed by the spreading of the ocean basin to a N-S width of ~1200 km by ~385 Ma.

Keywords: South China Block; Ailaoshan-Songma eastern Paleo-Tethys ocean (ASePTO); middle Devonian; paleomagnetism; paleogeographic reconstruction

Check for updates

Academic Editor: Urs Klötzli

Received: 22 June 2026
Revised: 25 July 2026
Accepted: 27 July 2026
Published: 29 July 2026

Copyright: © 2026 by the authors. Licensee MDPI, Basel, Switzerland. This article is an open access article distributed under the terms and conditions of the Creative Commons Attribution (CC BY) license.

1. Introduction

Over the past century, earth scientists have discovered that a unidirectional rifting and accretion geological process occurred within the Tethyan tectonic domain [1–5]. It is widely accepted that the opening of the Rheic Ocean between Avalonia and Gondwana during the Late Ordovician to Silurian-Devonian induced widespread tectonic extension along the northern margin of East Gondwana. Subsequently, during the Late Silurian to Early Devonian, a series of East Asian blocks progressively rifted away from Gondwana, marking the onset of the evolution of the eastern Paleo-Tethys Ocean [5–15]. However, robust quantitative constraints on the spatiotemporal evolution of the eastern Paleo-Tethys Ocean remain limited. Increasing evidence suggests that the kinematic evolution of the blocks within the eastern Paleo-Tethyan realm was likely more complex than previously recognized.

This study focuses on the rifting and drifting history of the South China Block (SCB) from Gondwana in order to constrain the timing of opening and subsequent spreading processes of the eastern Paleo-Tethys Ocean, particularly the Ailaoshan-Songma eastern Paleo-Tethys Ocean (ASePTO). On the one hand, according to the tectonic framework proposed by Zhao et al. [16], the East Asian blocks were likely involved in tectonic reorganization within the Proto- and Paleo-Tethyan domains following the breakup of Rodinia. Integrated geological and geophysical evidence from paleomagnetism, paleontology, and detrital zircon provenance records suggests that, by the Middle Ordovician, the SCB and associated East Asian blocks may have been amalgamated along the northern margin of Gondwana (Arabian-Indian-Australian sector) as a consequence of the subduction and closure of the Proto-Tethys Ocean. This tectonic configuration provides a fundamental constraint for investigating subsequent rifting of the SCB from Gondwana and the opening of the ASePTO. On the other hand, since the mid-Paleozoic, the SCB has occupied a critical tectonic position at the junction between the Tethyan and Pacific domains, where it preserves abundant and diverse geological records, making it a natural laboratory for studying Paleo-Tethyan tectonic evolution [17,18]. Therefore, the SCB represents an ideal target for investigating large-scale continental drift processes. A detailed study of its rifting history not only provides insights into the breakup of Gondwana and the subsequent accretion of Laurasia, but also helps to constrain the timing and geodynamic evolution of the eastern Paleo-Tethys Ocean. In addition, noting that paleomagnetism is currently the only geoscientific method capable of quantitatively or semi-quantitatively constraining kinematic processes of lithosphere plate/block, this study aims to provide key paleomagnetic constraints on critical tectonic intervals associated with the drift of Gondwana-derived blocks.

Existing paleomagnetic, geological, and paleontological evidence collectively indicates that the SCB was affiliated with East Gondwana during the Early Paleozoic. However, by the Late Carboniferous-Early Permian, the SCB and Gondwana exhibited markedly different sedimentary records, distinct biogeographic affinities, and significant paleolatitudinal separation, suggesting that they had already become rifted by that time [19]. Nevertheless, the timing and mechanism of the rifting of the SCB from Gondwana remain controversial, and the subsequent drifting processes are also poorly understood. Various studies generally offer the timing of the rifting of the SCB from Gondwana between the Late Ordovician and the Devonian [20–37].

From a paleomagnetism aspect, although only a limited number of Late Ordovician-Devonian paleomagnetic studies have been conducted on the SCB over the past several decades, available data constrain that the SCB was separated from Gondwana no later than the Devonian. Collectively, the Late Ordovician paleomagnetic pole [32] and the Middle to Late Silurian datasets [38,39] are characterized by well-constrained ages, relatively sufficient specimens, positive fold and reversal tests, and distinctive differences from any

younger poles. These Late Ordovician to Silurian paleopoles preliminarily indicate the SCB was located adjacent to Australia of East Gondwana by the end of the Silurian [33]. However, as reviewed by Huang et al. [33], the Devonian APWP for the SCB was almost unrestricted before this century due to the poor quality of a few preliminary data. Fortunately, this situation has significantly improved this century, with two studies [26,35] making encouraging progress. First, Zhang et al. [26] conducted a paleomagnetic study on the Devonian sequence from the Dushan-Pingtang area of Guizhou Province, and presented a few Devonian poles with positive reversals and consistency test results. More recently, Xian et al. [35] report a stable characteristic remanent component carried by hematite from the Middle Devonian Yuntaiguan Formation red beds in northwestern Hunan. This characteristic remanence successfully passed both fold and reversal tests and satisfies all seven reliability criteria of Van der Voo [40] and the updated criteria of Meert et al. [41], constraining the initiation of rifting and subsequent drifting of the SCB from Gondwana to approximately the Middle Devonian [35], which represents the earliest timing supported by reliable paleomagnetic evidence. However, this constraint should be regarded as a minimum bound rather than a definitive initiation age. Whether the separation of the SCB from Gondwana commenced prior to the Middle Devonian therefore remains unresolved, and the subsequent drifting history is still poorly constrained.

In this study, we report further new paleomagnetic data from Devonian sedimentary rocks of the SCB. By integrating the data with existing paleomagnetic, geological, and paleobiogeographic constraints, we reconstruct the paleogeographic evolution of the SCB and Gondwana, and evaluate the opening and spreading processes of the ASePTO.

2. Geological Setting and Paleomagnetic Sampling

The SCB, one of the largest cratonic units in eastern Asia, is characterized by a complex tectonic history. It is separated from the North China Block by the Qinling-Dabie-Sulu orogenic belt, while its northwestern margin is connected to the Songpan-Ganzi terrane via the Longmenshan-Qinghe fault system. To the southwest, the SCB is bounded by the Ailaoshan-Songma suture zone and is adjacent to the Indochina Block, whereas its southeastern margin faces the western Pacific realm. By the Middle to Late Silurian, large parts of the SCB were progressively uplifted, exposed subaerially, and subjected to erosion. Beginning in the Early Devonian, the SCB underwent a marine transgression originating from the southwest, gradually advancing northward and eastward, resulting in an onlap depositional pattern. Consequently, the Devonian strata system is only completely preserved in Guangxi. In regions such as Sichuan, Hubei, and Jiangxi, both the Lower Devonian and the lower part of the Middle Devonian are absent (Figure 1a). The Devonian strata in Guizhou Province are mainly distributed south of a line extending from Hezhang through Langjiacong, Zhijin, Zhujiaqiao, and Shibing to Rongjiang, which delineates a shallow-marine platform depositional zone [42–44].

Dushan County is located in southern Guizhou Province and belongs to the tectonic subdivision described above. The region is dominated by the Dushan box anticline, a Late Triassic fold [45,46], situated in the central part of the study area. The Devonian succession in the Dushan area has long attracted considerable attention owing to its exceptionally complete stratigraphic record and abundant paleontological remains. The stratigraphic framework, from the base upwards, comprises the Lower Devonian Danlin and Shujiaping formations; the Middle Devonian Longdongshui, Dahekou (Bangzhai), and Dushan formations; and the Upper Devonian Wangchengpo, Yaosuo, Zhewang, and Gelaohe formations (Figure 1c) [47–50]. Spatially, Lower to Middle Devonian strata are mainly exposed to the east of Dushan County, particularly in the Houershan area, whereas Upper Devonian units are preferentially developed to the west. Throughout the region, the Devonian is angularly

unconformable or disconformable in contact with the underlying Ordovician and Silurian strata (Figure 1b). The Lower Devonian deposits in the Dushan region consist of several hundred meters of deltaic-to-intertidal siliciclastic successions dominated by sandstones and siltstones, which host a diverse fossil assemblage of arthropods, fish, and early vascular plants, confirming the Early Devonian age for these strata [51]. In particular, the Danlin Formation is composed predominantly of grayish-white, medium- to thick-bedded quartz sandstones intercalated with thin layers of dark gray calcareous siltstone. It is conformably overlain by the Shujiaping Formation, which is characterized by dark purple to reddish, medium- to thick-bedded quartz sandstones alternating with thin-bedded calcareous and carbonaceous siltstones. The basal conglomeratic sandstone of the Shujiaping Formation serves as a key marker horizon, reflecting continuous sedimentation across the formation boundary. The Middle Devonian sections are typified by mixed carbonate-siliciclastic successions, in which member-scale subdivisions are primarily controlled by vertical fluctuations in terrigenous input and intraclastic components. Biostratigraphic constraints are provided by a characteristic brachiopod assemblage, including *Athyrisina squamosaeformis*, *Eospiriferina lachrymosa*, and *Acrospirifer houershanensis*, together with a rugose coral assemblage composed of *Utaratuia sinensis*, *Sociophyllum minor*, and *Dendrostella trigemme* from the Longdongshui Formation, indicating an Eifelian age [52]. The Dahekou Formation is dominated by yellowish, thick- to massive-bedded quartzose sandstones displaying well-developed cross-bedding structures and locally containing fossils of early terrestrial plants. These sedimentological characteristics suggest deposition in a nearshore environment. The development of the Dahekou Formation has been interpreted as a sedimentary response to the regional Haikou uplift event [53]. The Dushan Formation, first defined by Wenjiang Ding in 1929 and subsequently formalized in regional geological surveys [45], is well exposed in the study area. It is subdivided, in ascending order, into the Jipao (limestone-dominated), Songjiaqiao (sandstone-dominated), and Jiwozhai members (predominantly limestone or dolostones). Biostratigraphically, the Dushan Formation broadly corresponds to the *Bornhardtina-Stringocephalus* brachiopod Zone and is therefore assigned to the late Middle Devonian (Givetian) [54]. The Jiwozhai Member is composed mainly of reefal limestone and marly bedded limestone, with localized dolomitization, and contains a diagnostic rugose coral assemblage (*Endophyllum-Sunophyllum-Argutastrea*), further corroborating its Givetian age (Figure 1c) [54,55]. By contrast, the Upper Devonian strata in the Dushan region are dominated by shallow-marine dolostones, reflecting a distinct shift in depositional conditions relative to the underlying Middle Devonian successions.

Paleomagnetic sampling was systematically conducted at the formation or member level, with an average sampling location of 25.8° N/107.6° E. A total of nine oriented paleomagnetic site samples were collected from the Tunshang section: two sites (DL180-181) from the Danlin Formation, two sites (SJP182-183) from the Shujiaping Formation, and five sites (LDS184-188) from the Longdongshui Formation. The strata at this section exhibit a dip direction/dip of 198°/14° (right-hand strike/dip = 108°/14°). From the Lishan section, ten sites were sampled: five sites (DL199-203) from the Danlin Formation and five sites (SJP205-209) from the Shujiaping Formation, with a measured dip direction/dip of 160°/38°. The lithology at this section consists of highly pure quartz sandstone. At the Dahekou section, twenty-four sites (JP150-170, JP215-217) were collected from the Jipao Member, showing an average dip direction/dip of 308°/12°. The additional seven sites (JP143-149) from the same member were obtained from the Jipao section with an average dip direction/dip of 206°/14°. Seventeen sites (JWZ171-179, JWZ218-225) were sampled from the Jiwozhai Member at the Jinwozhai section, located adjacent to the high-speed railway line. These beds display an average dip direction/dip of 0°/10°. Finally, two sites (DS194-195) from the undivided Dushan Formation and three sites (LDS196-198) from

the Longdongshui Formation were collected at the Jiangzhai section, where the strata dip 143°/28°. A total of 72 sampling sites were established across 6 sections, and approximately 750 oriented core samples were collected. Statistical analysis of the stratigraphic attitudes of the sampling sections indicates a nonsignificant plunge of 0.1° of the fold axis.

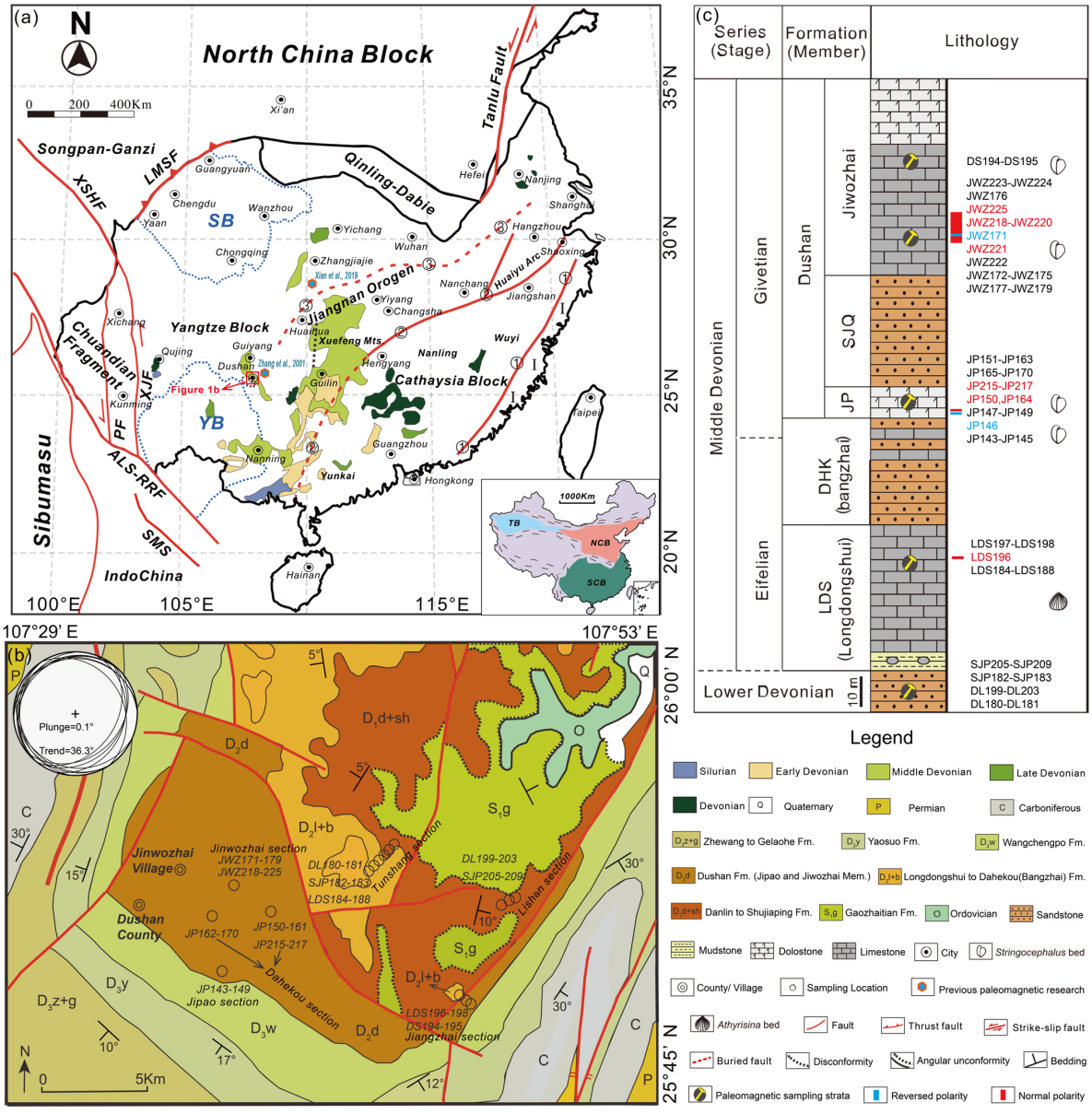


Figure 1. (**a**) The Silurian-Devonian sedimentary strata of the South China Block (SCB) in the schematic tectonics diagram (modified after Xian et al. [35]). The sampling locations of Devonian paleomagnetic studies (Zhang et al. [26], Xian et al. [35]) are denoted with a hexagon. Abbreviation: ALS-RRF (Ailaoshan–Red River Fault), SMS (Songma Suture), PF (Panzhihua Fault), XSHF-XJF (Xianshuihe–Xiaojiang Fault), LMSF (Longmenshan Fault), SB (Sichuan Basin), YB (Youjiang Basin), ① (Zhenghe–Dapu Fault Zone), ② (Shaoxing–Jiangshan–Pingxiang–Longsheng Fault Zone), ③ (Shitai–Jiujiang–Jishou Buried Fault Zone), I (Southeast China Coastal Magmatic Complex Zone) (according to Shu et al. [56]); (**b**) simplified geological map in Dushan area (modified after a 1:200,000 regional geological map of the Dushan sheet) [45], showing the locations of our paleomagnetic sampling sites with a stereonet of stratigraphic bedding attitude of the sampling sections from this study on the lower hemisphere; (**c**) schematic lithostratigraphic column illustrating Devonian strata in Dushan, showing the strata of the paleomagnetic specimens and the corresponding polarity (modified after Huang et al. [47–50]).

All cores were drilled with a portable petrol-powered drill, with in situ core orientations primarily determined via magnetic compass. A subset of cores was oriented using both magnetic and solar compasses and the average difference was 2.40° ± 0.52° (n = 242, 2σ). This offset is broadly consistent with the local geomagnetic declination of −2.74° predicted by the International Geomagnetic Reference Field (IGRF) model, indicating the magnetic compass readings could be effectively corrected by the IGRF local geomagnetic declination. Unfortunately, demagnetization trajectories of specimens from the Lower Devonian Danlin and Shujiaping formations do not exhibit systematic decay of remanence toward the origin and fail to yield the well-defined characteristic remanent magnetization (ChRMs), so these specimens were excluded for further discussion. The Longdongshui Formation specimens from the Middle Devonian Eifelian Stage exhibit an apparent Mesozoic remagnetization, which will be investigated in detail elsewhere and is not considered further in this study. Thus, only the experimental results from the Middle Devonian Givetian specimens, including the Jipao and Jiwozhai members of the Dushan Formation, and the undivided Dushan Formation, are discussed below.

3. Methods

3.1. Rock Magnetism

Rock magnetic experiments were conducted at the Magnetotectonics Laboratory of the School of Earth and Space Sciences, Peking University, and at the Oxford Magnetism Laboratory, University of Oxford. Acquisition of isothermal remanent magnetization (IRM) accompanied by complementary back-field demagnetization of saturation IRM and thermal demagnetization of three-axis IRMs (soft (<0.12 T), medium (0.12–0.4 T), and hard (0.4–2.0 T) coercivity fractions) was performed using an ASC IM-10-30 pulse magnetizer (ASC Scientific, Narragansett, DC, USA) and an JR-6A spinner magnetometer (AGICO, s.r.o., Brno, Czech Republic) [57,58]. Repeated temperature-dependent magnetic susceptibility (κ-T) experiments were carried out under an argon atmosphere, using incremental maximum peak temperatures at 250 °C, 350 °C, 400 °C, 450 °C, 550 °C, 620 °C, and 695 °C, respectively (designated as peak temperature-cycle hereafter), at an MFK1-FA multifunction kappabridge susceptibility meter equipped with a CS-4 temperature control system (AGICO, s.r.o., Brno, Czech Republic).

3.2. Demagnetization

The demagnetization strategy of ~8–12 specimens per site was adopted. The limestone specimens from the Middle Devonian successions, including the Jipao and Jiwozhai members of the Dushan Formation, and the undivided Dushan Formation, exhibited relatively weak natural remanent magnetization (NRM) intensities, generally on the order of ~10^{-2}–10^{-5} A/m. To effectively isolate ChRMs, a combination of three demagnetization approaches, progressive thermal demagnetization, alternating field (AF) demagnetization, and hybrid thermal/AF demagnetization, was employed by using a 2G Enterprises Model 755 cryogenic magnetometer (2G-RAPID system) (2G Enterprises, Sunnyvale, CA, USA) and PGL-100 demagnetization oven (Suzhou Grand Energy Technology Co., Ltd., Suzhou, China) [59] installed in magnetically shielded room with an average field intensity of ~170 nT in the paleomagnetic laboratory at the Institute of Tibetan Plateau Research, Chinese Academy of Sciences (ITPCAS). The hybrid demagnetization protocol consisted of three successive steps: (1) progressive thermal demagnetization up to 320 °C or 350 °C, (2) subsequent AF demagnetization to a maximum peak field of approximately 80 mT, and (3) a final reheating stage beginning at 360 °C. Thermal demagnetization was conducted with temperature increments of 50–100 °C at lower temperatures and 5–20 °C at higher temperatures. AF demagnetization was performed using a 2G600 AF degausser coupled

with a 2G755R cryogenic magnetometer (2G Enterprises, Sunnyvale, CA, USA), employing typical peak-field increments of 2–5 mT. The demagnetization results were plotted using orthogonal vector diagrams [60] and processed using principal component analysis (PCA) [61] to identify and isolate magnetic components. For each specimen, component direction was calculated using a minimum of four demagnetization steps. The Fisher statistics [62] were used to calculate mean remanence directions, carried out mainly with the software PMtools v.2.6.4 [63] and Pmagpy v.4.3.8 [64].

3.3. Petrographic Analysis

The optical petrography involved the transmitted plane-polarized light and reflected plane-polarized light in the thin sections. To further examine the magnetic properties, magnetic grain extraction was performed on the pilot limestone samples using a self-designed magnetic probe extraction apparatus [65], followed by scanning electron microscopy (SEM), transmission electron microscopy (TEM), and energy-dispersive X-ray spectroscopy (EDS) to identify the mineral composition, grain size, and morphology of the samples. Optical microscopy observations were conducted at the Optical Microscopy Laboratory, School of Earth and Space Sciences, Peking University. SEM/EDS analyses were performed at the Electron Microscopy Laboratory, School of Physics, Peking University. TEM/EDS analyses were conducted at the Electron Microscopy Laboratory, Institute of Geology and Geophysics, Chinese Academy of Sciences.

4. Results

4.1. Rock Magnetism Results

Representative Devonian samples, one to two selected from each sampled formation or member, were subjected to rock magnetic experiments described above. The IRM and three-axis IRM characteristics for the Middle Devonian, including Jipao and Jiwozhai members and undivided Dushan Formation, are nearly identical. These samples exhibit a rapid approach to IRM saturation within relatively low applied fields of approximately 200–300 mT (Figure 2a,d,g), indicating the predominance of low-coercivity magnetic minerals. The back-field demagnetization of SIRM yields B_{cr} with maximum values of up to ~100 mT, consistent with the dominance of ferrimagnetic minerals. The thermal demagnetization of the three-axis IRMs demonstrates that remanence in these samples is mainly carried by soft- to medium-coercivity components, with broadly distributed unblocking temperatures extending to ~450–550 °C (Figure 2b,e,h). Such unblocking behavior is a characteristic of fine-grained magnetite and/or maghemite. A rapid loss of remanence in both the medium and hard IRM components during the initial stages of thermal treatment suggests an additional presence of goethite.

The samples of Jipao and Jiwozhai members display nearly identical κ-T characteristics (e.g., JP150-10 and JWZ171-2, Figure 2c,f). Heating and cooling curves overlap below ~450 °C under argon, whereas the cooling curve of the 550-cycle shows significantly higher susceptibility than the heating curve, accompanied by a peak at ~240–280 °C. This behavior reflects the formation of pyrrhotite between ~450 and 550 °C, likely resulting from desulfurization of pyrite [66]. On the κ-T curves of the 620-cycle, the heating curve shows an abrupt susceptibility decrease after a peak at ~280–320 °C, again indicating pyrrhotite formation, while cooling curves lie well below heating curves, consistent with oxidation of maghemite to hematite for the surface partially oxidized [67]. The sharp susceptibility increase near ~320 °C on cooling after heating to ~695 °C corresponds closely to the Néel temperature of pyrrhotite and represents a diagnostic feature of this mineral [68]. The repeated κ-T experiments on the undivided Dushan Formation samples are characterized by heating and cooling curves that closely coincide below approximately 550 °C under

an argon atmosphere (e.g., DS195-5, Figure 2i). Above this temperature, cooling curves exhibit substantially higher susceptibility than heating curves, indicating the generation of fine-grained ferrimagnetic minerals during heating. The sharp susceptibility drops at ~550–580 °C on the heating κ-T curves of the 620-cycle and 695-cycle suggest that magnetite is the dominant magnetic carrier in the limestone of the undivided Dushan Formation.

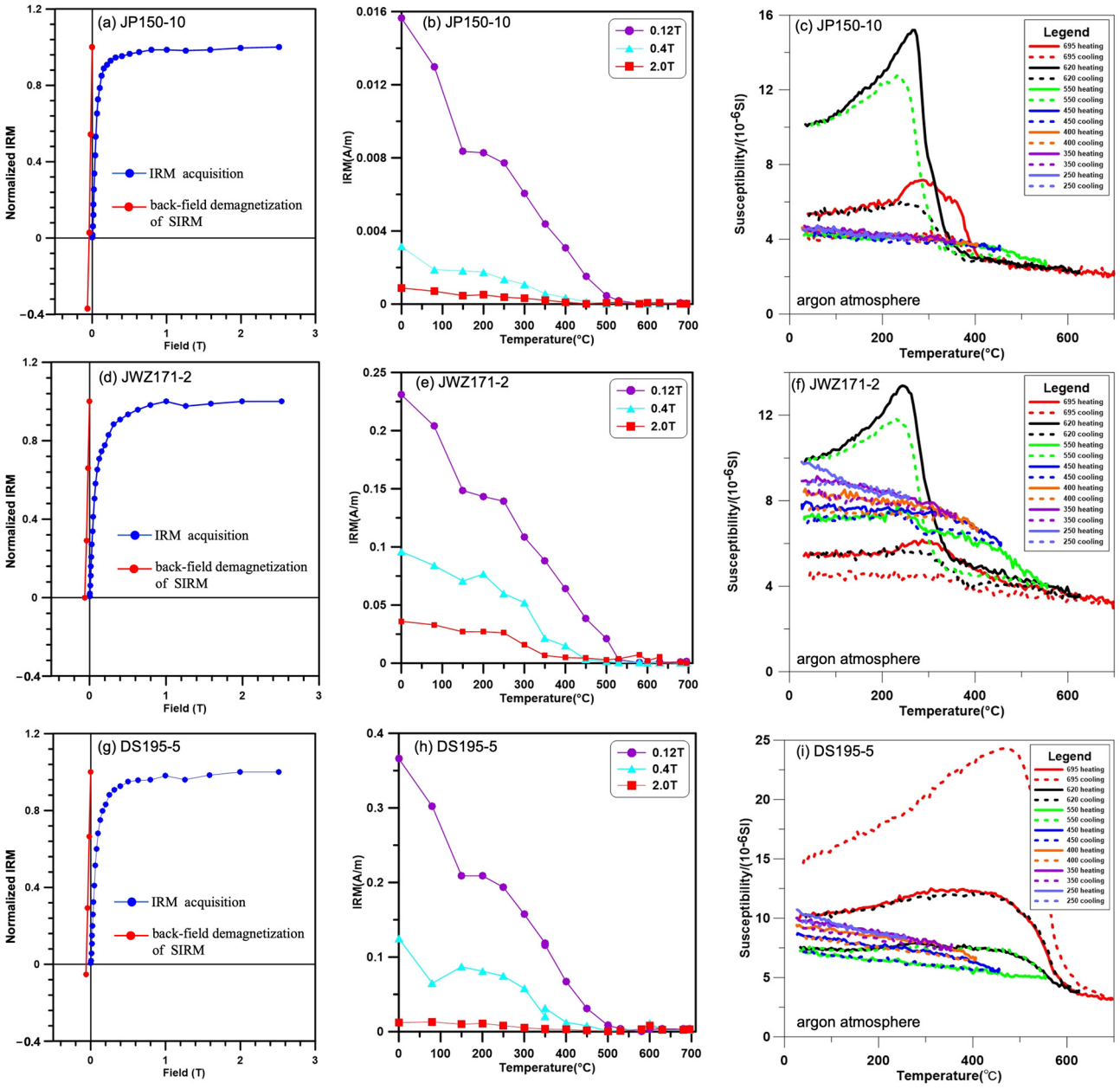


Figure 2. Behavior of isothermal remanent magnetization (IRM) acquisition and back-field demagnetization of saturation IRM (**a**,**d**,**g**), thermal demagnetization of three-axis IRMs (**b**,**e**,**h**), and multiple temperature cycles of κ-T curves (**c**,**f**,**i**) for samples from the Jipao and Jiwozhai members of the Dushan Formation, and the undivided Dushan Formation.

4.2. Demagnetization Results

The thermal, AF, and hybrid thermal/AF demagnetization experiments were conducted on limestone specimens from the Dushan Formation Jipao and Jiwozhai members, and the undivided Dushan Formation. These experiments yield the low-temperature/low-field components (LTCs/LFCs), unblocked below approximately 200–350 °C or under 5.0 mT peak AFs, and the high-temperature/high-field components (HTCs/HFCs), which

are generally isolated during an interval of ~200–3–50 °C to ~360–520 °C, or AF peak fields ranging from ~2.5–5.0 mT up to ~60–80 mT, and were designated as characteristic remanent magnetization (ChRM) hereafter.

Notably, limestone specimens from the Jipao Member consistently yield two distinct remanent magnetization components, i.e., the LTC/LFC and ChRM under all three demagnetization techniques (Figures 3a–f and S1a–h). In particular, a pair of parallel Jipao Member specimens (JP150-10A, B) was selected for comparative analysis: specimen JP150-10A was subjected exclusively to progressive thermal demagnetization, whereas specimen JP150-10B was treated using a combined protocol involving thermal, AF, and subsequent higher-temperature thermal demagnetizations. The resulting demagnetization trajectories obtained from the two approaches are essentially indistinguishable, indicating that the different demagnetization methods yield consistent and reproducible results for the Jipao Member limestones (Figure 3a,b). In contrast, although the majority of Jiwozhai Member specimens also yield two remanent magnetization components under all three demagnetization methods (Figures 3g,l,m and S1i–o), a subset of specimens displays only the single ChRM after the removal of a viscous component during the initial stage of demagnetization (Figure 3h–k). For the undivided Dushan Formation, two remanent magnetization components are generally resolved using progressive thermal and hybrid thermal/AF demagnetization methods (Figure S1p,r). However, AF demagnetizations typically isolate only the single high-field ChRM component (Figure S1q).

Overall, the LTCs/LFCs were successfully isolated from 302 out of the 417 demagnetized Givetian Dushan limestone specimens. As shown in Figure 4a,b, the in situ directions of these components cluster tightly around the Present Geomagnetic Field (PGF) direction (declination/inclination = −2.6°/40.5°) at the sampling location (25.8° N, 107.6° E). The Fisherian mean direction [62] is D_g/I_g = 352.7°/39.8° (α_{95} = 1.1°). Following the *tilt correction*, a pronounced deterioration in directional grouping is observed, as indicated by a k_s/k_g ratio of 0.44, indicating that the LTCs/LFCs represent a recently acquired secondary remagnetization. On the other hand, the ChRMs were isolated from 386 out of 417 demagnetized specimens. These ChRM directions are divided into two distinct groups, hereafter referred to as ChRM-A and ChRM-B. The ChRM-A yields a mean direction of D_g = 29.6°, I_g = 48.4° (k_g = 39.0, α_{95} = 1.3°, n = 321) before and D_s = 26.3°, I_s = 46.4° (k_s = 19.2, α_{95} = 1.8°, n = 321) after *tilt-correction* (Figure 4c,d; Table S1); whilst the ChRM-B is clustered by a mean direction of D_g = 45.3°, I_g = −20.0° (k_g = 30.9, α_{95} = 3.2°, n = 65) before and D_s = 48.8°, I_s = −22.5° (k_s = 24.6, α_{95} = 3.6°, n = 65) after *tilt-correction* (Figure 4e,f; Table S2).

The nature of the ChRM-A is easily reached by a series of fold tests. The ratio of precision parameters before and after the *tilt-correction* is k_g/k_s = 2.0408, which is significantly larger than the critical value F [640] = 1.15 at the 95% confidence level, indicating a negative fold test result [69]. Further using the bootstrap fold test implemented in the Python-based framework of Tauxe et al. [64] indicates that the ChRM-A attains optimal clustering within an unfolding range of −28% to 14% at the 95% confidence level. These fold test results indicate a secondary post-folding (i.e., the Dushan box-shaped anticline) nature for the ChRM-A. Noting the corresponding paleomagnetic pole of the in situ mean direction of the ChRM-A closely overlaps, within 95% confidence limits, with reported Mesozoic paleomagnetic poles from the SCB (Figure 4c,d), the ChRM-A should be a Mesozoic remagnetization.

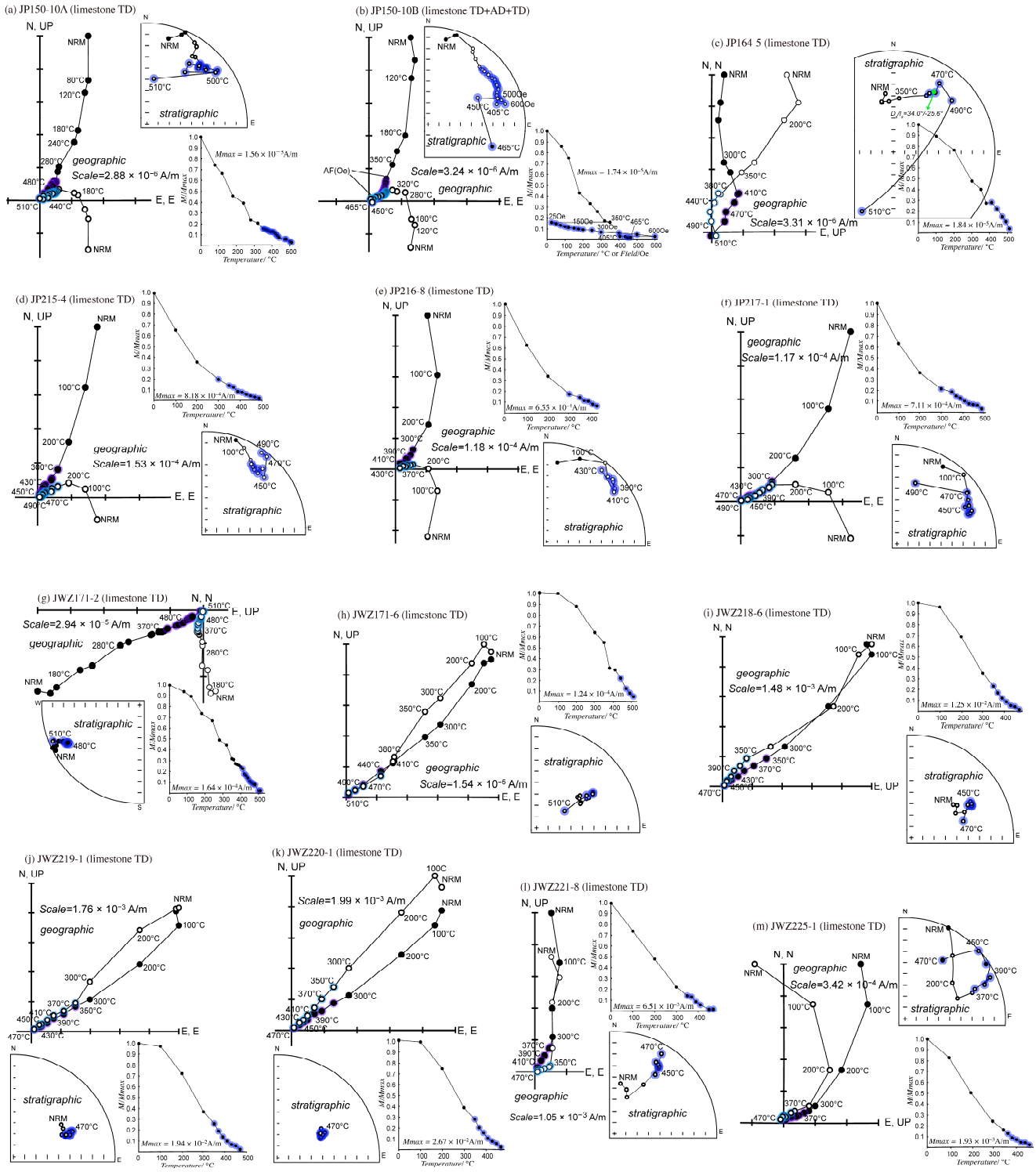


Figure 3. (**a**–**m**) Orthogonal vector plots and equal-area projections of representative limestone specimens from the Jipao and Jiwozhai members of the Dushan Formation. Most specimens were subjected to thermal demagnetization, such as specimens JP150-10A, JWZ171-2 and JWZ225-1. A small subset of specimens adopted a hybrid demagnetization protocol, including JP150-10B. Solid and open circles in orthogonal plots (all drawn in situ) indicate vector endpoints projected onto the horizontal and vertical planes, whereas solid and open circles in equal-area projections (all plotted after *tilt-correction*) represent directions plotted onto lower and upper hemispheres, respectively. The colored circles represent the points involved in the calculation of the ChRM-B by the PCA and the fitted direction, while the non-colored circles correspond to the low-temperature components (LTCs) and/or viscous overprint in the initial stage of the demagnetization.

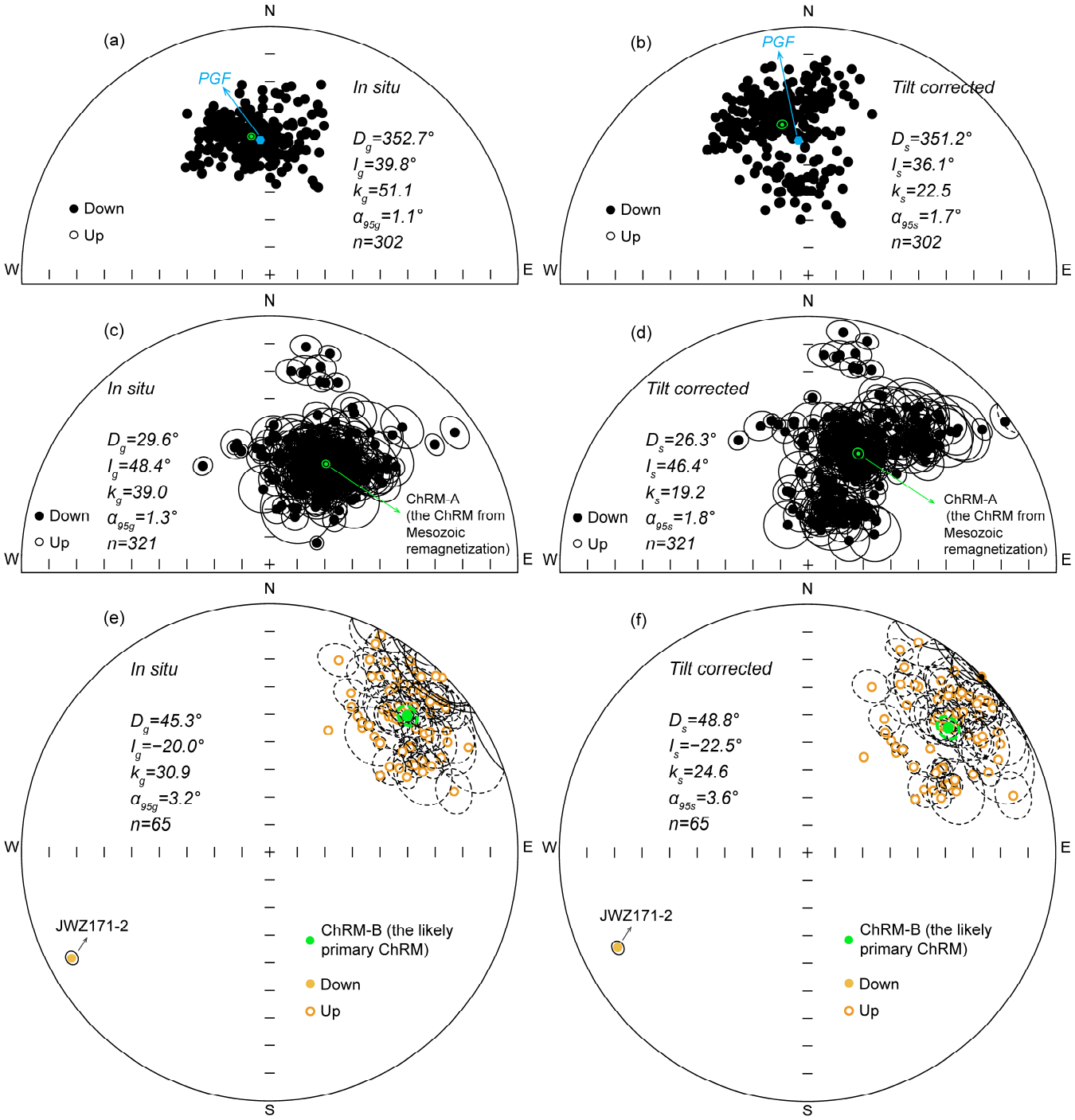


Figure 4. Equal-area projections of specimen-mean directions of (**a**,**b**) the low-temperature/low-field components (LTCs/LFCs), (**c**,**d**) ChRM-A, and (**e**,**f**) ChRM-B isolated from Givetian Dushan limestone specimens before (**a**,**c**,**e**) and after (**b**,**d**,**f**) the *tilt-correction*. The green circle stands for the mean direction; the blue hexagon represents the local Present Geomagnetic Field (PGF) direction. The rest follow Figure 3.

In contrast, for the ChRM-B, although there is a slight deterioration of the data grouping after the *tilt-correction* (k_s/k_g = 0.80), either the McElhinny [69] classical fold test (k_g/k_s = 1.25 < F [128] = 1.34 at the 95% confidence) or the McFadden [70] fold test (ξ_2 = 20.67 in situ and ξ_2 = 36.36 in stratigraphic coordinates, with a critical value of ξ_c = 9.38 at the 95% confidence) yields an inconclusive test result. We interpret this inclusive fold test as a result of the monoclinic nature of the sampled stratigraphic sections

and the relatively minor variation in bedding attitudes within sampling sites/sections. The ChRM-B is dominated by normal polarity, characterized by northeast-directed declinations and shallow upward inclinations. Reversed polarity (i.e., southwest-directed declination with shallow downward inclination) was observed in only one specimen (JWZ171-2). Owing to the limited number of reversed-polarity data, a formal reversals test is not meaningful. Nevertheless, the paleopoles derived from the ChRM-B, both before and after *tilt-correction*, are distinctly different from the post-Middle Devonian poles of the SCB, suggesting that the ChRM-B most likely represents a primary remanence acquired during the Middle Devonian (Figure 4e,f; Table S4). Its primary origin is discussed in detail below.

4.3. Petrographic Results

To further constrain the magnetic mineralogy and remanence carriers of the Middle Devonian limestone specimens, petrographic observations were conducted on thin sections of representative limestone samples (JWZ171-7, JP215-11, JP217-2, and JWZ218-6) from the Jipao and Jiwozhai members using optical microscopy. Iron oxide and iron sulfide minerals were systematically examined. Iron sulfides, identified as pyrite based on their bright brassy reflections and speckled appearance, occur in two principal morphologies. Pyrite is predominantly present as framboidal aggregates (Figure 5e,o), with a subordinate occurrence as euhedral crystals (Figure 5f,g). The most abundant magnetic phase observed in the samples is pyrite that has undergone partial oxidation and replacement by iron oxides. The presence of brownish yellow-orange to reddish-brown reflections along grain margins and within grain interiors suggests that the oxidation products of pyrite are primarily fine-grained goethite and/or pigmentary hematite (Figure 5e–h,m–p) [71]. These oxidation-derived goethite and/or pigmentary hematite phases occur in minor abundances and are characterized by weak chemical remanent magnetization (CRM). As a result, they produce only a very weak response in rock magnetic measurements and demagnetization experiments.

Detailed observations of magnetic-extracted limestone samples (JP216-1 and JWZ218-2) were carried out using SEM coupled with EDS. Secondary electron (ETD) imaging reveals the widespread occurrence of spherical particles (Figure 6a–d). Many of these spherules exhibit smooth surfaces with worm-like textures, and EDS analyses indicate that they are composed predominantly of iron oxides. In some incompletely developed spherules (Figure 6a), minor amounts of magnesium (Mg) and sodium (Na) were detected, suggesting that clay minerals may have released iron during dehydration and subsequent illitization processes, thereby contributing to the formation of these iron oxide spherules.

To further constrain the magnetic mineralogy, grain-size distribution, morphological characteristics, and origin of the magnetic carriers in the limestones of the Jipao and Jiwozhai members of the Dushan Formation, TEM observations were conducted on magnetic extracts from representative limestone samples (JWZ225-5 and JP150-12). The results indicate that the magnetic particles in the limestones range from nanometer- to micrometer-scale and fall within the single-domain to multidomain (SD-MD) grain-size spectrum. A comprehensive characterization of the nanoscale magnetic particles was performed using bright-field imaging (BF), high-resolution transmission electron microscopy (HRTEM), selected-area electron diffraction (SAED), and EDS, allowing the microstructural features and mineral compositions of the magnetic carriers to be identified. Magnetic particles extracted from the Jiwozhai Member display detrital morphologies, characterized by angular crystal edges with limited abrasion. Grain sizes predominantly range from 50 to 130 nm (Figure 7a,d). HRTEM and SAED analyses reveal the presence of nanoscale maghemite (Figure 7b,c) and magnetite (Figure 7e,f) particles. Corresponding EDS spectra show enrichment in Fe and O, accompanied by abundant Si and minor Ti (Figure 7i). These observations

suggest that the nanoscale maghemite and magnetite particles are most likely hosted as inclusions within detrital silicate minerals such as plagioclase and pyroxene [72]. Such detrital magnetic inclusions are capable of carrying stable remanent magnetization [73,74]. This interpretation is consistent with the SEM observations presented above, which show partial illitization of silicate minerals in the incompletely developed spherical magnetic grains (Figure 6a,m). The occurrence of nanoscale maghemite also provides a mineralogical explanation for the thermal demagnetization behavior of the Jiwozhai limestone specimens, which exhibit a broad unblocking temperature spectrum and a decay of remanence intensity to near the noise level between 400 and 500 °C. Magnetic particles extracted from the Jipao Member similarly display detrital morphologies, with grain sizes ranging from 70 to 170 nm (Figure 7g,h). EDS analyses yield results comparable to those of the Jiwozhai Member, with Fe and O as the dominant elements, accompanied by abundant Si and minor Ti (Figure 7i). These results indicate that the nanoscale magnetite particles are likewise of detrital origin and possess the capacity to retain the likely primary stable remanent magnetization. In addition, recent micromagnetic simulations have also demonstrated that magnetite grains within the size range mentioned above can effectively preserve primary remanent magnetization [75–77].

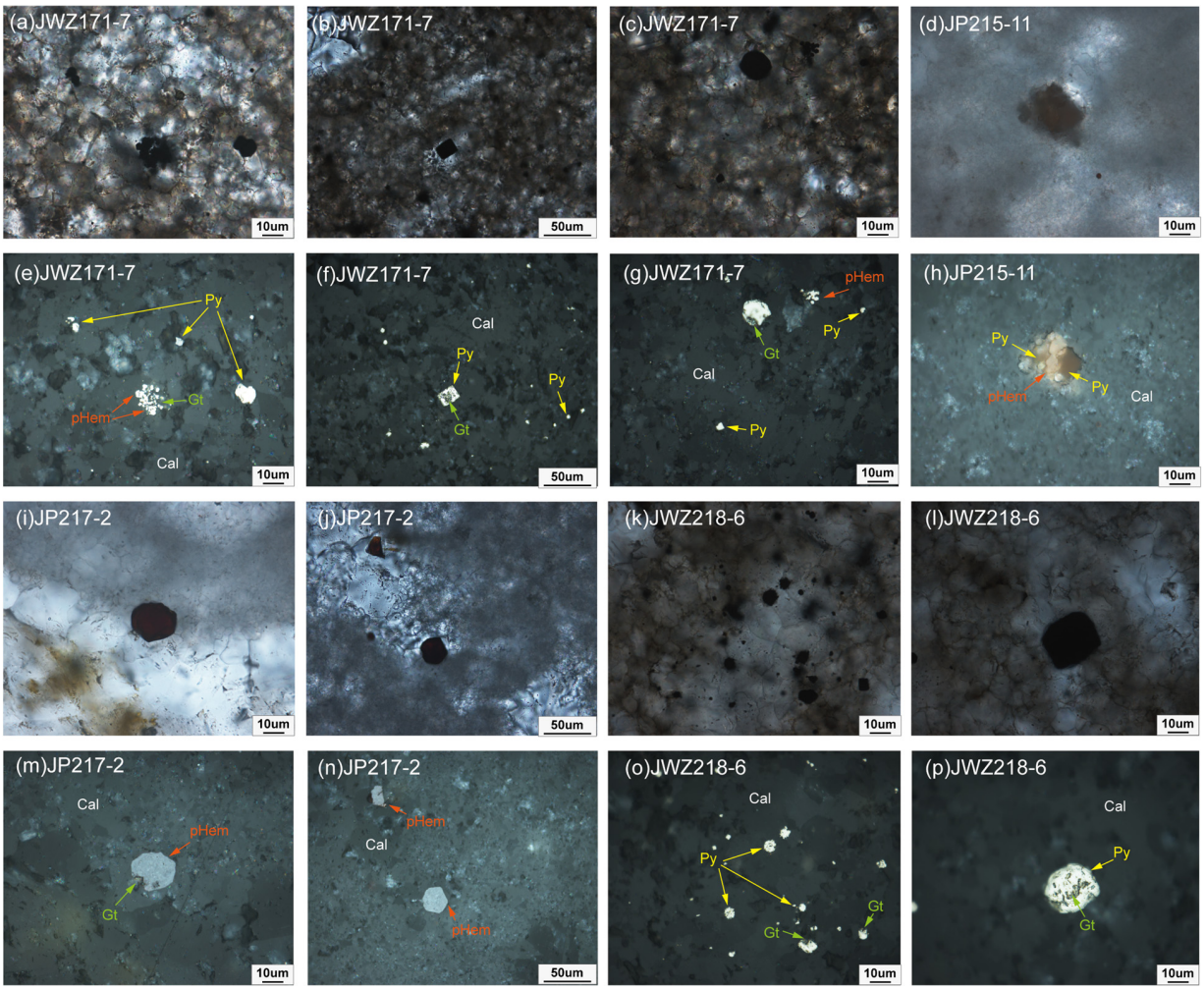


Figure 5. The optical microscopy illustrating the iron oxide and iron sulfide minerals of limestones from the Jipao and Jiwozhai members of the Dushan Formation. Panels (**a**–**d**) and (**i**–**l**) show the results obtained under transmitted plane-polarized light, whilst panels (**e**–**h**) and (**m**–**p**) correspond to the results under reflected plane-polarized light. pHem = pigmentary hematite; Gt = goethite; Py = pyrite; Cal = calcite.

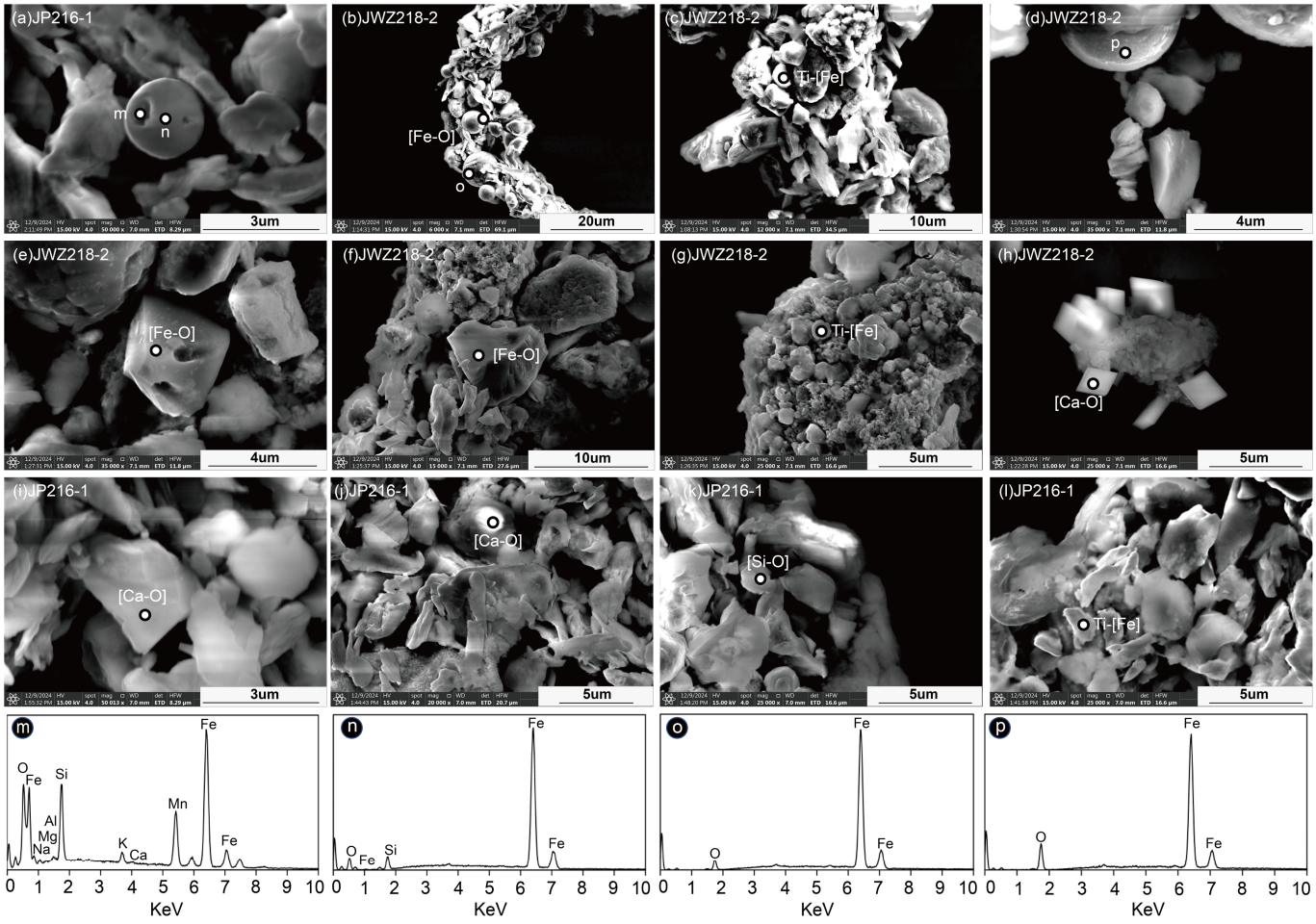


Figure 6. (**a**–**l**) Scanning electron microscopy (SEM) and (**m**–**p**) energy-dispersive X-ray spectroscopy (EDS) analyses of the magnetic extracts from the limestones of the Jipao and Jiwozhai members of the Dushan Formation. The EDS spectra shown in panels (**m**,**n**) correspond to specimen JP216-1 in panel (**a**); the EDS spectrum in panel (**o**) is derived from specimen JWZ218-2 in panel (**b**); the EDS spectrum in panel (**p**) corresponds to specimen JWZ218-2 in panel (**d**).

Collectively, the SEM/EDS and TEM/EDS observations indicate that the oxidation products of framboidal and euhedral pyrite are most likely pigmentary hematite and/or goethite rather than magnetite, which are generally regarded as ineffective carriers of remanent magnetization and therefore contribute little to the preservation of primary ChRMs [78]. In contrast, the primary ChRMs in the Jipao and Jiwozhai members of the Dushan Formation limestones are inferred to be predominantly carried by nanoscale detrital magnetite and maghemite. It should be noted, however, that magnetite and maghemite were not directly identified in the present optical microscopy or SEM/EDS analyses. This absence is most plausibly attributed to its very low abundance and fine grain size, which likely fall below the detection limits of these techniques. HRTEM analyses enabled the effective identification of these nanoscale magnetic and maghemite minerals. Integrating mineralogical morphology and compositional characteristics, systematic demagnetization results, and previously published micromagnetic modeling constraints, we infer that the limestones of the Jipao and Jiwozhai members of the Dushan Formation are capable of carrying stable primary remanent magnetization. The ChRM-B isolated from the demagnetization experiments is therefore most likely to represent a primary remanence signal.

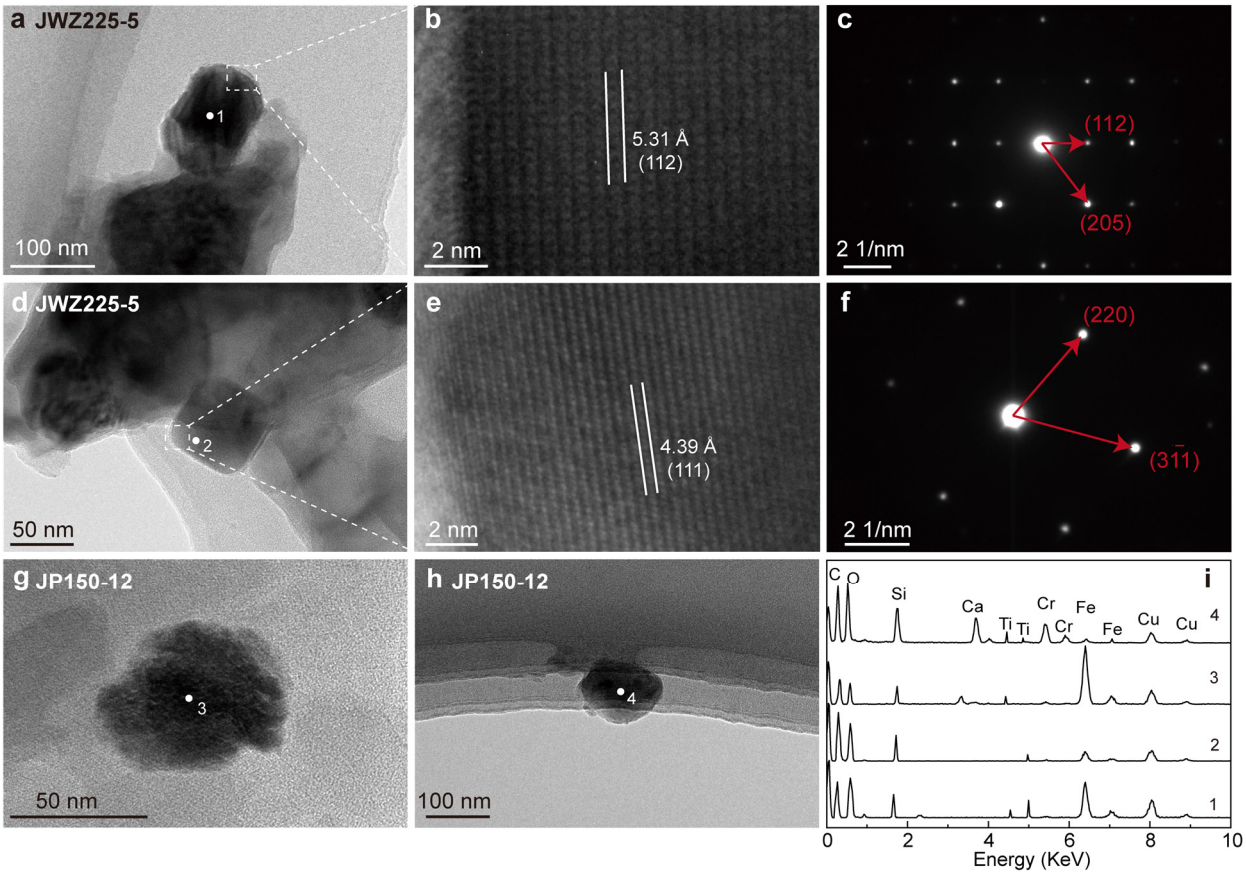


Figure 7. Transmission electron microscopy (TEM) and EDS analyses of magnetic extracts from limestones of the Jipao and Jiwozhai members of the Dushan Formation. (**a**,**d**) Bright-field (BF) TEM images of the Jiwozhai Member limestone magnetic extract (sample JWZ225-5); (**b**,**e**) high-resolution transmission electron microscopy (HRTEM) images of sample JWZ225-5; (**c**,**f**) selected-area electron diffraction (SAED) patterns of sample JWZ225-5; (**g**,**h**) BF TEM images of the Jipao Member limestone magnetic extract (sample JP150-12); (**i**) EDS results for magnetic extracts from both the Jipao and Jiwozhai members. The numbers 1–4 and white dots mark the positions of EDS spot measurements.

5. Discussion

5.1. Origin of the Characteristic Remanent Magnetizations (ChRMs)

Given the post-folding origin of the ChRM-A and the close correspondence between the corresponding paleomagnetic pole calculated from the in situ mean direction (63.6° N, 183.0° E; dp/dm = 1.1°/1.7°) and the Early-Middle Jurassic reference poles of the SCB [79–82]; the ChRM-A is inferred to be an Early-Middle Jurassic remagnetization acquired probably in response to the formation of the Dushan box-shaped anticline.

The ChRM-B is mainly derived from limestone specimens collected from two relatively gently dipping short sections (each approximately 1–2 m thick) of the Jipao and Jiwozhai members (Figure S2a–d). Rock magnetic experiments, together with optical microscopy, SEM/EDS and TEM/EDS observations, indicate that nanoscale detrital magnetite and maghemite are the dominant magnetic carriers of this component. The oxidation products of framboidal and euhedral pyrite are most likely hematite and/or goethite rather than magnetite [78], and therefore do not contribute significantly to the remanent magnetization. Notably, the paleomagnetic pole calculated from *tilt-corrected* ChRM-B (29.5° N, 229.8° E; dp/dm = 2.0°/3.8°; Table S2) is distinct from all published SCB paleopoles younger than the Middle Devonian, but is consistent with the Middle Devonian reference pole of the SCB (Figure 8) [26,35]. Overall, we believe the ChRM-B is very likely to represent a primary remanent magnetization.

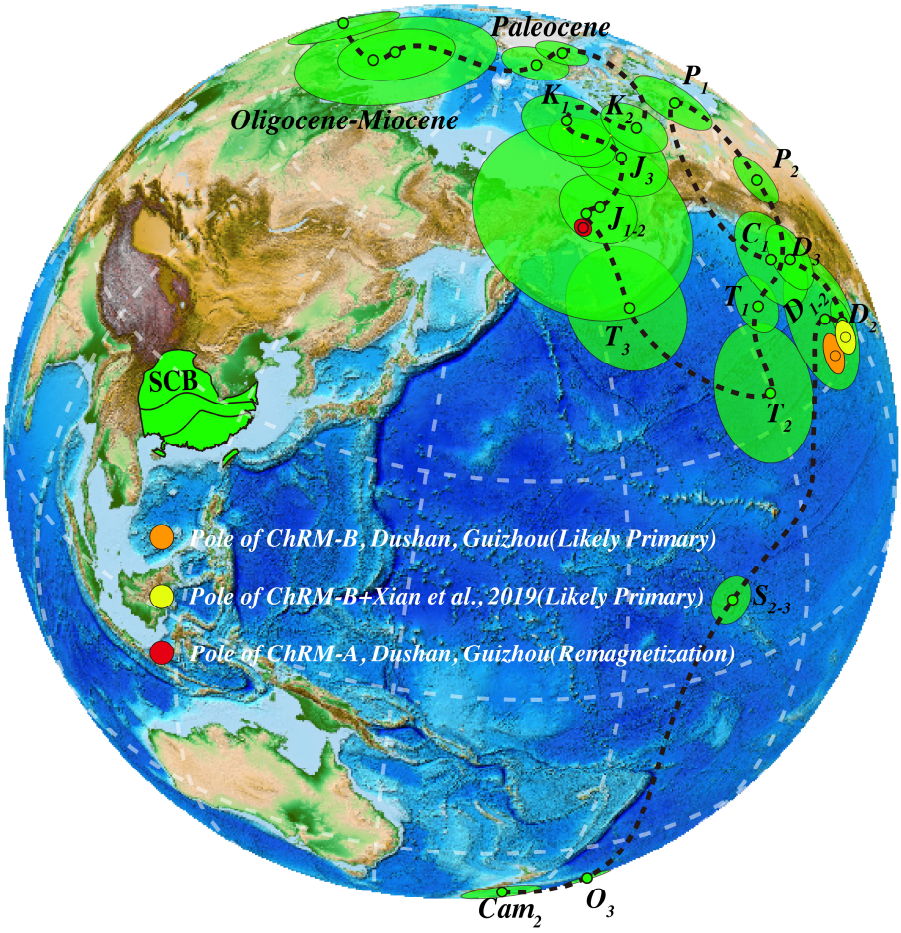


Figure 8. The poles (solid color circles) derived from the primary and remagnetized components of the Middle Devonian specimens are plotted on the apparent polar wander path (APWP) of the SCB [26,27,80–94]. The poles derived from the primary ChRM-B and ChRM-B + Xian et al. [35] do not coincide with any younger paleopoles of the SCB. Cam, O, S, D, C, P, T, J, K denote the Cambrian, Ordovician, Silurian, Devonian, Carboniferous, Permian, Triassic, Jurassic and Cretaceous periods, with 1 = Early, 2 = Middle, and 3 = Late. The black dashed line represents the APWP of the SCB.

5.2. Rationale for Combining the ChRM-B and Yuntaiguan Formation Dataset

To obtain a more robust Middle Devonian Givetian Stage paleomagnetic pole for the SCB, we evaluated whether the newly obtained ChRM-B directions could be combined with previously published coeval paleomagnetic data from western Hunan [35]. For this, a direct comparison was made between the two datasets (Table S3). Since the data of Xian et al. [35] consists of site-mean directions, the ChRM-B data were pre-processed to ensure comparability by averaging adjacent specimens into site-mean directions. Following this procedure, seven composite sites were defined: JP150, JWZ171, JP215, JP216, JP217, JWZ221, and a combined site consisting of specimens from sampling site JWZ218, 219, 220, and 225. One specimen (JP164-5, Figure 3c) was excluded from this analysis because no adjacent specimens were available for site-level averaging. The recalculated site-mean ChRM-B directions from the Jipao and Jiwozhai members of the Dushan Formation show not only an apparent consistent distribution of normal and reversed polarities with the Middle Devonian data reported by Xian et al. [35] (Figure 9a,b), but also a statistical consistency between them. As shown in Figure 9c, application of Watson's modified V_w statistics resulted in V_w = 5.4, which is well below the corresponding critical value (V_{crit} = 7.5) [95].

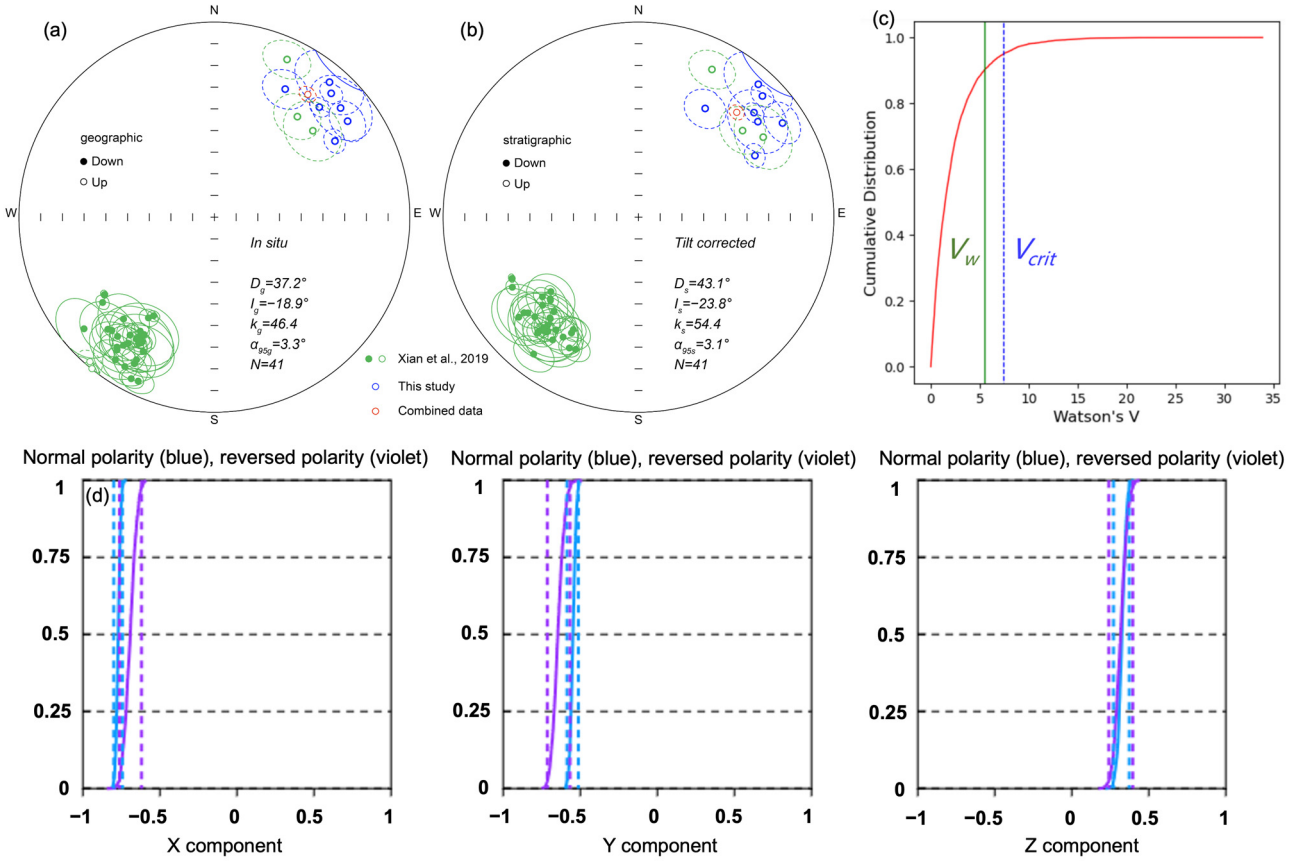


Figure 9. (**a**,**b**) Equal-area stereographic projection of the combined site-mean ChRMs before and after the *tilt-correction*. Open (solid) circles are projections on the upper (lower) hemisphere; (**c**) distribution of Watson's V_w for the combined site-mean ChRMs simulated using the Pmagpy Python software package (Pmagpy v.4.3.8, Available online: https://earthref.org/PmagPy/ (accessed on 25 May 2026)). V_w (the solid green line) is not larger than the V_{crit} value (the dashed blue line), proving that the two datasets are not significantly different [95]. The solid red line represents the cumulative distribution of Watson's V derived from Monte Carlo simulations; (**d**) bootstrap reversals test showing that, in the 95% confidence limits, the combined site-mean ChRMs passing the reversals test within the 95% confidence limit. The region between the two dashed lines denotes the 95% confidence limits. The solid line represents the cumulative distribution curve of directional data obtained from Monte Carlo simulations.

Beyond the statistical consistency, both sampling locations lie within the interior of the SCB and are not separated by any first-order tectonic boundary. No evidence exists for independent local and/or regional vertical-axis rotation, major strike-slip faults, or terrane boundaries between them [96]. Thus, both statistical and geological evidence indicates that the ChRM-B from Givetian Dushan Formation limestones in Guizhou could be combined with those isolated from coeval Yuntaiguan Formation red beds in Hunan (Xian et al., 2019) [35] to provide a more robust paleomagnetic reference pole for the SCB. The combined site-mean ChRM directions yield a mean of D_g/I_g = 37.2°/−18.9°, k_g = 46.4, α_{95} = 3.3°; D_s/I_s = 43.1°/−23.8°, k_s = 54.4, α_{95} = 3.1°, N = 41 (Figure 9a,b; Table S3). Using the fold test of McFadden [70], the critical value was calculated as ξ_c = 7.45 at the 95% confidence limit, while the observed statistics yielded ξ_2 = 12.63 in situ and ξ_2 = 6.11 after the *tilt-correction*, indicating a positive fold test result for this combined site-mean ChRMs; meanwhile, a bootstrap reversals test [97], implemented using PmagPy [64], shows that all three components of the combined site-mean ChRMs intersect within the 95% confidence limits, indicating also a positive reversals test (Figure 9d). Collectively, these remanence

stability tests demonstrate that the combined site-mean ChRMs have a pre-folding origin and are very likely primary magnetizations acquired at, or close to, the time of deposition.

In addition, noting that the Middle Devonian red beds of the Yuntaiguan Formation do not suffer significant compaction-induced inclination shallowing [35], consistent with their low clay content, formation in low-latitude regions near the paleoequator, and the absence of pronounced elongation in directional distribution. The consistency between the ChRMs isolated from the Givetian limestones from southern Guizhou and those from coeval Yuntaiguan red beds [35] in western Hunan further supports the inference that sedimentary compaction effects on magnetic inclination were minimal in low-latitude equatorial settings during the Middle Devonian.

During the Early Devonian, the geomagnetic field is characterized by mixed polarity, with reversed polarity being dominant. In contrast, normal polarity prevailed during the Eifelian, whereas the polarity pattern in the late Eifelian and throughout the Givetian Stage remains poorly known [98,99]. The combined ChRM directions are characterized by northeast declinations with shallow upward inclinations, accompanied by a number of antipodal directions, suggesting acquisition during different geomagnetic polarity intervals. Paleontological constraints indicate that the SCB occupied low paleolatitudes near the paleoequator, but preferentially within the Southern Hemisphere, from the Early Paleozoic through the Middle Devonian [19,37,100,101]. When considered together with previously proposed paleopoles of the SCB, such as O_3 [32], $S_{2–3}$ [38,39], and $D_{1–2}$ [26,28], and constrained using the shortest polar wander principle in APWP construction (Figure 8), the southwest declinations with shallow downward-inclinations are interpreted as records of reversed polarity intervals, whereas the northeast declinations with shallow upward-inclinations are records of normal polarity intervals.

Accordingly, a new and robust key reference pole, located at 33.2° N, 234.7° E with A_{95} = 2.4° and with a median age of ~385 Ma, is assigned to the Middle Devonian SCB. It places the SCB at low paleolatitudes of the Southern Hemisphere during the Givetian, corresponding to a paleolatitude of ~12.4°S for the Dushan sampling location (25.8° N, 107.6° E). This paleopole is clearly distinct from any younger published poles of the SCB (Figure 8; Table S4; Text S1).

5.3. Paleogeographic Implications

To place the rifting and drifting of the SCB from Gondwana within the spatiotemporal framework of tectonic evolution in the eastern Tethyan domain, the newly obtained Middle Devonian (Givetian Stage) paleomagnetic data were integrated with previously published, high-quality anchor or quasi-primary paleomagnetic poles of the SCB spanning approximately 510–320 Ma. These reference poles were selected based on both Q-values [40] and R-values [41] exceeding 4, and, in particular, on reliable isotopic or biostratigraphic age controls [26,27,32,33,35,38,39,82,102]. The compiled dataset includes, but is not limited to, paleomagnetic results from Upper Ordovician Baota Formation limestones [32], Lower-Middle Silurian sandstones [91], Middle-Upper Silurian siltstones [38], Silurian red beds [39], Lower-Middle Devonian limestones and sandstones [26], and Upper Devonian limestones and sandstones (Table S5) [26]. All datasets incorporated into this compilation are characterized by well-constrained stratigraphic ages and sufficient numbers of independently oriented specimens. In addition, the ChRMs from these studies passed established primary stability tests, and the resulting paleomagnetic poles are demonstrably distinct from younger poles reported for the SCB, supporting their interpretation as primary or quasi-primary records of the Paleozoic geomagnetic field.

A sliding-window averaging and spline interpolation method was applied to the selected paleomagnetic data to generate a mathematically derived APWP, thereby interpo-

lating and bridging temporal gaps in the data record. The refined SCB dataset was then used to construct a detailed APWP spanning the Middle Cambrian to Late Carboniferous and was compared with the coeval synthesized APWP of the Gondwana continent for the same period (Table S6) [103], thereby providing a framework to constrain the timing and kinematic process of the opening of the ASePTO under paleomagnetic constraints.

The updated Paleozoic APWP of the SCB aligns with that of Gondwana when it was clockwise rotated by ~73.5° about an Euler pole at 5.7° N, 122.1° E, overlapping with the early Paleozoic APWP of Gondwana in a fixed African reference frame. This suggests that the SCB remained connected to East Gondwana from the Middle Cambrian to Early Devonian (~510–410 Ma), with its southeastern margin located adjacent to northwestern Australia (Figure 10a), and the SCB has been located near the paleoequator since the early Paleozoic. After ~410 Ma, the APWP of the SCB diverges distinctly from that of Gondwana. At this time, Gondwana itself underwent a large-scale clockwise rotation, and its Devonian-Carboniferous APWP follows a great circle; whereas the Devonian-Carboniferous APWP of the SCB trends in the opposite direction. This indicates that the SCB may have begun to rift from East Gondwana during the late Early Devonian (~410–400 Ma), resulting in a gradual opening of the ASePTO between them (Figure 10a,b). After ~400 Ma, as Gondwana continued its rapid southward migration toward high southern latitudes, the SCB remained near the paleoequator while the ASePTO between the SCB and Gondwana continued to spread, reaching a latitudinal width of ~1200 km (~11.5°) by ~385 Ma (Figure 10c), consistent with the paleogeographic reconstructions of the SCB proposed by Golonka [104].

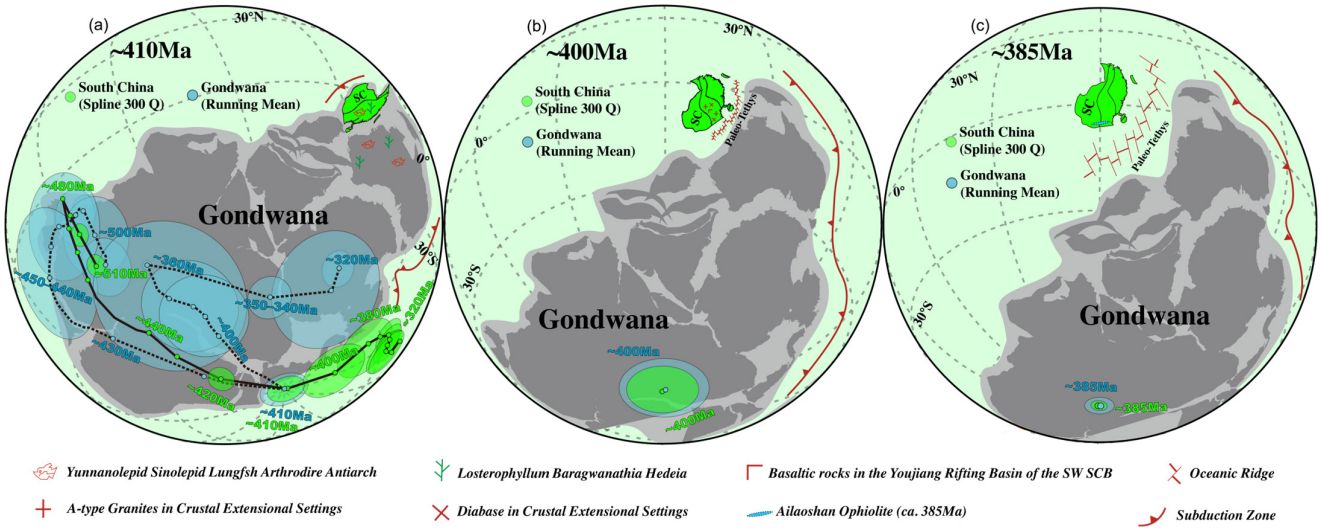


Figure 10. Paleogeographic reconstructions of the SCB relative to Gondwana in a fixed African reference frame at (**a**) ~410 Ma, (**b**) ~400 Ma, and (**c**) ~385 Ma. The fit of Gondwana is mainly modified after Torsvik et al. [103] and is marked with blue circles. The SCB poles are marked as green circles. The ages of all number-labeled paleopoles are in Ma. Paleomagnetic south poles were used in the plotting. See Table S6 for more details [19,25,29–31,37,103–107].

These paleogeographic reconstructions, mostly based on paleomagnetic data, are further supported by a series of geological and paleontological evidence, which can be summarized as follows: (i) Sedimentary and oceanic evidence from the Youjiang Basin. A series of studies have suggested that rifting of the SCB from Gondwana during the late Early Devonian may have triggered the initial opening of the Paleo-Tethys Ocean in the Youjiang Basin (Guangxi). This process is documented by the development of deep-marine depositional systems and the occurrence of radiolarian-bearing siliceous rocks, indicative of oceanic basin formation [25,29–31]. (ii) Paleontological correlations. Comparative analyses of Devonian fossil fish assemblages from Qujing (Yunnan, South China) and Australia

demonstrate strong biogeographic affinities, leading to the inference that separation of the SCB from Gondwana had occurred no later than the Middle Devonian [37]. (iii) Extensional tectonics and coeval magmatism. During the Early-Middle Devonian, the Youjiang Basin was characterized by NW-trending extensional sub-basins and NE-trending strike-slip fault systems. These tectonic processes were accompanied by the eruption of basalts in the late Early Devonian, which are widely interpreted to record the initial stage of lithospheric extension associated with SCB-Gondwana rifting [25,105]; and (iv) Intraplate magmatism within the SCB. The timing of SCB-Gondwana separation broadly coincides with the emplacement of crustal extension-related A-type granitoids and diabase intrusions within the SCB. These magmatic events, dated to ~415–400 Ma, provide further support for an Early Devonian onset of rifting [106,107].

6. Conclusions

The paleomagnetic result obtained in this study, together with previously published paleomagnetic data from the SCB spanning ~510–320 Ma, leads to the following principal conclusions.

1. A new primary characteristic remanence (ChRM-B) was isolated from the Givetian (~385 Ma) limestones of the Jipao and Jiwozhai members of the Dushan Formation from southern Guizhou of the SCB. The primary origin is supported by (i) its corresponding paleomagnetic pole (29.5° N, 229.8° E; $dp/dm = 2.0°/3.8°$) showing distinctively different from all previously reported post-Middle Devonian poles from the SCB; (ii) rock magnetic analyses and high-resolution transmission electron microscopy (HRTEM) observations indicating the ChRM-B is predominantly carried by nanoscale detrital magnetite and maghemite; and (iii) compatibility with the published coeval primary remanence from the Yuntaiguan Formation red beds in western Hunan.
2. A combination of the primary ChRM-B from the Dushan limestones in southern Guizhou with those reported from the coeval Yuntaiguan Formation red beds in western Hunan yields a robust Givetian key reference pole at 33.2° N, 234.7° E ($A_{95} = 2.4°$; R = 7) for the SCB, based on 41 site-mean directions. The combined dataset passes both reversals and fold tests and indicates the SCB was located at a low paleolatitude of ~12.4°S during the Givetian.
3. By incorporating the newly established robust Givetian paleopole with previously well-constrained Paleozoic poles, a revised Paleozoic APWP for the SCB was constructed using a sliding-window averaging approach combined with spline interpolation. Comparison between the Paleozoic APWPs of the SCB and Gondwana indicates that a prolonged tectonic linkage between them existed from the Middle Cambrian to the Early Devonian (~510–410 Ma), followed by progressive rifting during the late Early Devonian. Continued drifting during the Middle Devonian resulted in a fundamental paleogeographic reorganization, whereby the SCB remained near the paleoequator while Gondwana migrated rapidly toward higher southern latitudes. This divergence led to substantial widening of the ASePTO by ~385 Ma, providing critical constraints on the timing and kinematics of SCB-Gondwana breakup.

Supplementary Materials: The following supporting information can be downloaded at: https://www.mdpi.com/article/10.3390/min16080793/s1, Table S1: The ChRM-A of the Jipao and Jiwozhai members of the Dushan Formation, and the undivided Dushan Formation; Table S2: The ChRM-B of the Jipao and Jiwozhai members of the Dushan Formation; Table S3: Site-mean ChRM directions from the Givetian Jipao and Jiwozhai limestones of the Dushan Formation (reference location: 25.8° N, 107.6° E) and the Yuntaiguan Formation in NW Hunan of Xian et al. [35]. All the ChRM directions from Xian et al. [35] were transformed to the Dushan sampling location for comparison;

Table S4: Comparison of paleomagnetic pole obtained in this study with the reference APWP of the SCB to determine whether the pole (in this study) is likely primary; Table S5: Summary of available Paleozoic to Early Carboniferous paleomagnetic north poles for the SCB; Table S6: APWPs for the SCB and Gondwana. The SCB APWP is calculated using the spherical spline method with a smoothing factor of 300 and input poles weighted by their Q-factor according to the data in Table S5, whilst the Gondwana APWP is calculated using a running mean path with a 20 Ma sliding window from Torsvik et al. [103]; Figure S1: Orthogonal vector plots and equal-area projections of the thermal, alternating field (AF) and hybrid thermal/AF demagnetization results of representative likely remagnetized specimens from the Jipao and Jiwozhai members of the Dushan Formation and undivided Dushan Formation. Solid and open circles in orthogonal plots (all drawn in situ) indicate vector endpoints projected onto the horizontal and vertical planes, respectively, while solid and open circles in equal-area projections (all plotted in situ) represent directions plotted onto lower and upper hemispheres, respectively. The colored circles represent the points involved in the calculation of the ChRM-A by the PCA and the fitted direction; whereas the non-colored circles almost correspond to the LTCs/LFCs; Figure S2: Representative paleomagnetic sampling sections of the Middle Devonian in the Dushan area of the SCB; Text S1: The quality criteria for paleomagnetic data.

Author Contributions: Conceptualization, writing—original draft, Y.L. and B.H.; writing—reviewing and editing, Y.L., B.H., C.I.O.N. and D.L.; investigation, Y.L., B.H., Z.C., Z.L., E.Z. and Z.Y.; visualization, Y.L., R.H., Q.S. and D.L.; supervision, B.H., C.I.O.N. and Y.Y.; funding acquisition, B.H. All authors have read and agreed to the published version of the manuscript.

Funding: This research was funded by the National Natural Science Foundation of China (NSFC), Grant/Award Number: 92055205.

Data Availability Statement: All data generated and analyzed during this study are included in this published article.

Acknowledgments: The authors are grateful to the paleomagnetic laboratory at the Institute of Tibetan Plateau Research, Chinese Academy of Sciences (ITPCAS), and the Oxford Magnetism Laboratory, University of Oxford, for the use of their facilities.

Conflicts of Interest: The authors declare no conflicts of interest.

Abbreviations

The following abbreviations are used in this manuscript:

SCB	South China Block
ASePTO	Ailaoshan-Songma eastern Paleo-Tethys Ocean
IGRF	International Geomagnetic Reference Field
ChRMs	Characteristic Remanent Magnetizations
IRM	isothermal remanent magnetization
NRM	natural remanent magnetization
AF	alternating field
PCA	principal component analysis
APWP	apparent polar wander path
CRM	chemical remanent magnetization
SEM	Scanning Electron Microscopy
TEM	transmission electron microscopy
EDS	energy-dispersive X-ray spectroscopy
LTCs/LFCs	low-temperature/low-field components
HTCs/HFCs	high-temperature/high-field components
PGF	Present Geomagnetic Field
BF	bright-field
HRTEM	high-resolution transmission electron microscopy
SAED	selected-area electron diffraction

References

1. Storey, B.C. The role of mantle plumes in continental breakup: Case histories from Gondwanaland. *Nature* **1995**, *377*, 301–308. [CrossRef]
2. Stampfli, G.M.; Hochard, C.; Vérard, C.; Wilhem, C.; von Raumer, J. The formation of Pangea. *Tectonophysics* **2013**, *593*, 1–19. [CrossRef]
3. Torsvik, T.H.; Cocks, L.R.M. Gondwana from top to base in space and time. *Gondwana Res.* **2013**, *24*, 999–1030. [CrossRef]
4. Lawver, L.A.; Norton, I.O.; Dalziel, I.W.D.; Davis, M.D. *The Plates 2020 Atlas of Plate Reconstructions (500 Ma to Present Day)*; Tech. Rep. No. 238; University of Texas Institute for Geophysics: Austin, TX, USA, 2020; p. 29.
5. Torsvik, T.H.; Cocks, L.R.M. Devonian. In *Earth History and Palaeogeography*; Cambridge University Press: Cambridge, UK, 2016; pp. 138–158. [CrossRef]
6. Stampfli, G.M.; Borel, G.D. A plate tectonic model for the Paleozoic and Mesozoic constrained by dynamic plate boundaries and restored synthetic oceanic isochrons. *Earth Planet. Sci. Lett.* **2002**, *196*, 17–33. [CrossRef]
7. Murphy, J.B.; Gutierrez-Alonso, G.; Nance, R.D.; Fernandez-Suarez, J.; Keppie, J.D.; Quesada, C.; Strachan, R.A.; Dostal, J. Origin of the Rheic Ocean: Rifting along a Neoproterozoic suture? *Geology* **2006**, *34*, 325–328. [CrossRef]
8. Von Raumer, J.F.; Stampfli, G.M. The birth of the Rheic Ocean—Early Palaeozoic subsidence patterns and subsequent tectonic plate scenarios. *Tectonophysics* **2008**, *461*, 9–20. [CrossRef]
9. Nance, R.D.; Gutiérrez-Alonso, G.; Keppie, J.D.; Linnemann, U.; Murphy, J.B.; Quesada, C.; Strachan, R.A.; Woodcock, N.H. A brief history of the Rheic Ocean. *Geosci. Front.* **2012**, *3*, 125–135. [CrossRef]
10. Nance, R.D.; Gutiérrez-Alonso, G.; Keppie, J.D.; Linnemann, U.; Murphy, J.B.; Quesada, C.; Strachan, R.A.; Woodcock, N.H. Evolution of the Rheic Ocean. *Gondwana Res.* **2010**, *17*, 194–222. [CrossRef]
11. Torsvik, T.H.; Cocks, L.R.M. The Palaeozoic palaeogeography of central Gondwana. *Geol. Soc. Lond. Spec. Publ.* **2011**, *357*, 137–166. [CrossRef]
12. Dan, W.; Murphy, J.; Wang, Q.; Zhang, X.Z.; Tang, G.J. Tectonic evolution of the Proto-Qiangtang Ocean and its relationship with the Palaeo-Tethys and Rheic oceans. *Geol. Soc. Lond. Spec. Publ.* **2022**, *531*, 249–264. [CrossRef]
13. Neubauer, F.; Liu, Y.; Dong, Y.; Chang, R.; Genser, J.; Yuan, S. Pre-Alpine tectonic evolution of the Eastern Alps: From Prototethys to Paleotethys. *Earth-Sci. Rev.* **2022**, *226*, 103923. [CrossRef]
14. Golonka, J.; Khuong The, H.; Nguyen, D.; Krobicki, M. The eastern extension of the Avalonian terranes, the Prototethys and Paleotethys oceans. *Geotour. Geotur.* **2023**, *20*, 72–73. [CrossRef]
15. Pastor-Galán, D.; López-Carmona, A.; Rezaeian, M.; Tsujimori, T.; Gutiérrez-Alonso, G.; Yi, K.; Langereis, C. From Rheic to Paleotethys: Subduction history of the Shanderman eclogites (NW Iran). *GSA Bull.* **2025**, *137*, 4478–4496. [CrossRef]
16. Zhao, G.; Wang, Y.; Huang, B.; Dong, Y.; Li, S.; Zhang, G.; Yu, S. Geological reconstructions of the East Asian blocks: From the breakup of Rodinia to the assembly of Pangea. *Earth-Sci. Rev.* **2018**, *186*, 262–286. [CrossRef]
17. Wang, Y.; Fan, W.; Zhang, G.; Zhang, Y. Phanerozoic tectonics of the South China Block: Key observations and controversies. *Gondwana Res.* **2013**, *23*, 1273–1305. [CrossRef]
18. Zhang, G.; Guo, A.; Wang, Y.; Li, S.; Dong, Y.; Liu, S.; He, D.; Cheng, S.; Lu, R.; Yao, A. Tectonics of South China continent and its implications. *Sci. China Earth Sci.* **2013**, *56*, 1804–1828. [CrossRef]
19. Metcalfe, I. Gondwana dispersion and Asian accretion: Tectonic and palaeogeographic evolution of eastern Tethys. *J. Asian Earth Sci.* **2013**, *66*, e33. [CrossRef]
20. Young, G. Devonian vertebrate distribution patterns and cladistic analysis of palaeogeographic hypotheses. *Geol. Soc. Lond. Mem.* **1990**, *12*, 243–255. [CrossRef]
21. Young, G. Biogeography of Devonian vertebrates. *Alcheringa* **1981**, *5*, 225–243. [CrossRef]
22. Stöcklin, J. The Tethys paradox in plate tectonics. In *Plate Reconstruction from Paleozoic Paleomagnetism*; American Geophysical Union: Washington, DC, USA, 1984; pp. 27–28. [CrossRef]
23. Burrett, C.; Long, J. Early-Middle Palaeozoic biogeography of Asian terranes derived from Gondwana. *Geol. Soc. Lond. Mem.* **1990**, *12*, 163–174. [CrossRef]
24. Van der Voo, R. *Paleomagnetism of the Atlantic, Tethys and Iapetus Oceans*; Cambridge University Press: Cambridge, UK, 1993. [CrossRef]
25. Xun, Z.; Allen, M.B.; Whitham, A.G.; Price, S.P. Rift-related Devonian sedimentation and basin development in South China. *J. Southeast Asian Earth Sci.* **1996**, *14*, 37–52. [CrossRef]
26. Zhang, S.; Zhu, H.; Meng, X. New paleomagnetic results from the Devonian-Carboniferous successions in the southern Yangtze Block and their paleogeographic implications. *Acta Geol. Sin.* **2001**, *75*, 311–313. (In Chinese with English abstract) [CrossRef]
27. Yang, Z.; Sun, Z.; Yang, T.; Pei, J. A long connection (750–380 Ma) between South China and Australia: Paleomagnetic constraints. *Earth Planet. Sci. Lett.* **2004**, *220*, 423–434. [CrossRef]

28. Zhang, S. South China's Gondwana connection in the Paleozoic: Paleomagnetic evidence. *Prog. Nat. Sci.* **2004**, *14*, 85–90. [CrossRef]
29. Du, Y.; Hu, H.; Huang, Z.Q.; Xu, Y.; Yang, J.; Huang, H. Basin translation from Late Paleozoic to Triassic of Youjiang Basin and its tectonic significance. *Geol. Sci. Technol. Inf.* **2009**, *28*, 10–15. (In Chinese with English abstract)
30. Du, Y.; Huang, H.; Yang, J.; Huang, H.; Tao, P.; Huang, Z.; Hu, L.; Xie, C. The basin translation from Late Paleozoic to Triassic of the Youjiang Basin and its tectonic signification. *Geol. Rev.* **2013**, *59*, 1–11. (In Chinese with English abstract)
31. Hara, H.; Kurihara, T.; Kuroda, J.; Adachi, Y.; Kurita, H.; Wakita, K.; Hisada, K.; Charusiri, P.; Charoentitirat, T.; Chaodumrong, P. Geological and geochemical aspects of a Devonian siliceous succession in northern Thailand: Implications for the opening of the Paleo-Tethys. *Palaeogeogr. Palaeoclimatol. Palaeoecol.* **2010**, *297*, 452–464. [CrossRef]
32. Han, Z.; Yang, Z.; Tong, Y.; Jing, X. New paleomagnetic results from Late Ordovician rocks of the Yangtze Block, South China, and their paleogeographic implications. *J. Geophys. Res.-Solid Earth* **2015**, *120*, 4759–4772. [CrossRef]
33. Huang, B.; Yan, Y.; Piper, J.D.A.; Zhang, D.; Yi, Z.; Yu, S.; Zhou, T. Paleomagnetic constraints on the paleogeography of the East Asian blocks during Late Paleozoic and Early Mesozoic times. *Earth-Sci. Rev.* **2018**, *186*, 8–36. [CrossRef]
34. Liu, H.; Xia, X.; Lai, C.K.; Gan, C.; Zhou, Y.; Huang, F. Break-away of South China from Gondwana: Insights from the Silurian high-Nb basalts and associated magmatic rocks in the Diancangshan-Ailaoshan fold belt (SW China). *Lithos* **2018**, *318–319*, 194–208. [CrossRef]
35. Xian, H.; Zhang, S.; Li, H.; Xiao, Q.; Chang, L.; Yang, T.; Wu, H. How did South China connect to and separate from Gondwana? New paleomagnetic constraints from the Middle Devonian red beds in South China. *Geophys. Res. Lett.* **2019**, *46*, 7371–7378. [CrossRef]
36. Qiu, L.; Yan, D.P.; Tang, S.L.; Chen, F.; Song, Z.D.; Gao, T.; Zhang, Y.X. Insights into post-orogenic extension and opening of the Palaeo-Tethys Ocean recorded by an Early Devonian core complex in South China. *J. Geodyn.* **2020**, *135*, 101708. [CrossRef]
37. Wang, J.; Mi, Y.; Ma, X.; Bi, Y. Stratigraphic correlation of the Givetian (late Middle Devonian) deposits in Qujing, Yunnan, southwestern China and the paleogeographic implications. *Turk. J. Earth Sci.* **2022**, *31*, 284–293. [CrossRef]
38. Opdyke, N.D.; Huang, K.; Xu, G.; Zhang, W.Y.; Kent, D.V. Paleomagnetic results from the Silurian of the Yangtze paraplatform. *Tectonophysics* **1987**, *139*, 123–132. [CrossRef]
39. Huang, K.; Opdyke, N.D.; Zhu, R. Further paleomagnetic results from the Silurian of the Yangtze Block and their implications. *Earth Planet. Sci. Lett.* **2000**, *175*, 191–202. [CrossRef]
40. Van der Voo, R. The reliability of paleomagnetic data. *Tectonophysics* **1990**, *184*, 1–9. [CrossRef]
41. Meert, J.G.; Pivarunas, A.F.; Evans, D.A.D.; Pisarevsky, S.A.; Pesonen, L.J.; Li, Z.; Elming, S.-Å.; Miller, S.R.; Zhang, S.; Salminen, J.M. The magnificent seven: A proposal for modest revision of the Van der Voo (1990) quality index. *Tectonophysics* **2020**, *790*, 228549. [CrossRef]
42. Bureau of Geology and Mineral Resources of Guizhou Province. *Regional Geology of Guizhou Province*; Geological Publishing House: Beijing, China, 1987. (In Chinese)
43. Bureau of Geology and Mineral Resources of Guizhou Province. *Regional Geology of Guizhou Province*; Geological Publishing House: Beijing, China, 2013. (In Chinese)
44. Jin, S.Y.; Ju, T.Y. *Distribution Characteristics, Genesis and Reservoir Property of Sinian-Triassic Reefs in South China*; Shanghai Scientific and Technical Press: Shanghai, China, 1998. (In Chinese with English abstract)
45. No. 108 Geological Survey Team, Guizhou Bureau of Geology. *Regional Geological Survey Report of the Dushan Sheet (1:200,000), People's Republic of China (G-48-XXIV, Geological Section)*; Guizhou Bureau of Geology: Guiyang, China, 1965. (In Chinese)
46. Yang, X.Y.; Li, X.Q.; Huang, L. Distribution regularity and prospecting significance of sulfur-rich iron deposits in Dushan area of Guizhou. *Guizhou Geol.* **2016**, *33*, 8–13. (In Chinese with English abstract)
47. Huang, J.; Kershaw, S.; Liang, K.; Qie, W. The South China Block: A reef-building focal point in Givetian (Middle Devonian) of eastern Palaeotethys. *Earth-Sci. Rev.* **2025**, *269*, 105202. [CrossRef]
48. Huang, J.; Kun, L.; Wang, Y.; Kershaw, S.; Jeon, J.; Li, Y.; Qie, W. Stromatoporoids from a Middle Devonian reef of South China and their palaeoecological implication. *Acta Palaeontol. Pol.* **2022**, *67*, 711–736. [CrossRef]
49. Huang, J.; Li, Y.; Kershaw, S.; Liang, K.; Qie, W. Middle Devonian sequence changes impacting reef growth in southern Guizhou, South China Block. *J. Asian Earth Sci.* **2023**, *248*, 105618. [CrossRef]
50. Huang, J.; Liang, K.; Wang, Y.; Liao, W.; Guo, W.; Kershaw, S.; Jeon, J.; Qiao, L.; Song, J.; Ma, J.; et al. The Jiwozhai patch reef: A palaeobiodiversity hotspot in middle Givetian (Devonian) of South China. *Palaeogeogr. Palaeoclimatol. Palaeoecol.* **2020**, *556*, 109895. [CrossRef]
51. Huang, P.; Liu, L.; Xue, J.Z. A new polysporangiate land plant with novel fertile organs from the Lower Devonian of Guizhou, southwestern China. *Rev. Palaeobot. Palynol.* **2022**, *302*, 104661. [CrossRef]
52. Liao, W.H.; Deng, Z.Q. Age re-assessment of the Longdongshui Member (Middle Devonian) in southern Guizhou on the basis of benthic fossils. *Acta Palaeontol. Sin.* **2009**, *48*, 637–645. (In Chinese with English abstract)

53. Hou, H.F. Devonian strata in South China. In *Symposium on the Devonian Strata of South China*; Institute of Geology and Mineral Resources, Chinese Academy of Geological Sciences, Ed.; Geological Publishing House: Beijing, China, 1978; pp. 214–230. (In Chinese with English abstract)
54. Liao, W.H. Devonian biostratigraphy of Dushan, southern Guizhou and its coral extinction events. *Acta Palaeontol. Sin.* **2003**, *42*, 417–427. (In Chinese with English abstract)
55. Liao, W.H.; Ma, X.P. On the Givetian transgression in South China and the Endophyllum-bearing beds—With a comparison of Endophyllum from South China and "Endophyllum" from northern Xinjiang. *Acta Palaeontol. Sin.* **2011**, *50*, 64–76. (In Chinese with English abstract)
56. Shu, L.; Yao, J.; Wang, B.; Faure, M.; Charvet, J.; Chen, Y. Neoproterozoic plate tectonic process and Phanerozoic geodynamic evolution of the South China Block. *Earth-Sci. Rev.* **2021**, *216*, 103596. [CrossRef]
57. Lowrie, W. Identification of ferromagnetic minerals in a rock by coercivity and unblocking temperature properties. *Geophys. Res. Lett.* **1990**, *17*, 159–162. [CrossRef]
58. Muttoni, G.; Kent, D.V.; Orchard, M. Paleomagnetic reconnaissance of early Mesozoic carbonates from Williston Lake, northeastern British Columbia, Canada: Evidence for late Mesozoic remagnetization. *Can. J. Earth Sci.* **2001**, *38*, 1157–1168. [CrossRef]
59. Qin, H.; Zhao, X.; Liu, S.; Paterson, G.A.; Jiang, Z.; Cai, S.; Li, J.; Liu, Q.; Zhu, R. An ultra-low magnetic field thermal demagnetizer for high-precision paleomagnetism. *Earth Planets Space* **2020**, *72*, 170. [CrossRef]
60. Zijderveld, J.D.A.A.C. demagnetization of rocks: Analysis of results. In *Developments in Solid Earth Geophysics*; Collinson, D.W., Creer, K.M., Runcorn, S.K., Eds.; Elsevier: Amsterdam, The Netherlands, 1967; Volume 3, pp. 254–286. [CrossRef]
61. Kirschvink, J.L. The least-squares line and plane and the analysis of palaeomagnetic data. *Geophys. J. Int.* **1980**, *62*, 699–718. [CrossRef]
62. Fisher, R.A. Dispersion on a sphere. *Proc. R. Soc. Lond. A-Math. Phys. Eng. Sci.* **1953**, *217*, 295–305. [CrossRef]
63. Efremov, I.; Veselovskiy, R. PMTools: New application for paleomagnetic data analysis. *Izv. Phys. Solid Earth* **2023**, *59*, 798–805. [CrossRef]
64. Tauxe, L.; Shaar, R.; Jonestrask, L.; Swanson-Hysell, N.L.; Minnett, R.; Koppers, A.A.P.; Constable, C.G.; Jarboe, N.; Gaastra, K.; Fairchild, L. PmagPy: Software package for paleomagnetic data analysis and a bridge to the Magnetics Information Consortium (MagIC) database. *Geochem. Geophys. Geosyst.* **2016**, *17*, 2450–2463. [CrossRef]
65. Zhao, Q. Reconnaissance of the Paleogeography of the India-Asia Collision. Ph.D. Thesis, Peking University, Beijing, China, 2021.
66. Li, H.; Zhang, S. Detection of mineralogical changes in pyrite using measurements of temperature-dependence susceptibilities. *Chin. J. Geophys.* **2005**, *48*, 1454–1461. (In Chinese with English abstract) [CrossRef]
67. Dunlop, D.J. Magnetism in rocks. *J. Geophys. Res.-Solid Earth* **1995**, *100*, 2161–2174. [CrossRef]
68. Wang, L.; Pan, Y.; Li, J.; Qin, H. Rock magnetic investigation of the thermal transformation of pyrite. *Sci. China Ser. D-Earth Sci.* **2008**, *38*, 1068–1077. (In Chinese)
69. McElhinny, M.W. Statistical significance of the fold test in palaeomagnetism. *Geophys. J. Int.* **1964**, *8*, 338–340. [CrossRef]
70. McFadden, P. A new fold test for paleomagnetic studies. *Geophys. J. Int.* **1990**, *103*, 163–169. [CrossRef]
71. Zhao, Q.; Huang, B.; Yi, Z.; Xue, P. High-resolution petrographic evidence confirming detrital and biogenic magnetites as remanence carriers for Zongpu carbonates in the Gamba area, South Tibet. *Front. Earth Sci.* **2021**, *9*, 713469. [CrossRef]
72. Chang, L.; Roberts, A.; Heslop, D.; Hayashida, A.; Li, J.; Zhao, X.; Tian, W.; Huang, Q. Widespread occurrence of silicate-hosted magnetic mineral inclusions in marine sediments and their contribution to paleomagnetic recording: Magnetic inclusions in marine sediments. *J. Geophys. Res.-Solid Earth* **2016**, *121*, 8415–8431. [CrossRef]
73. Tarduno, J.A.; Cottrell, R.D.; Watkeys, M.K.; Bauch, D. Geomagnetic field strength 3.2 billion years ago recorded by single silicate crystals. *Nature* **2007**, *446*, 657–660. [CrossRef] [PubMed]
74. Tarduno, J.A.; Cottrell, R.D.; Watkeys, M.K.; Hofmann, A.; Doubrovine, P.V.; Mamajek, E.E.; Liu, D.; Sibeck, D.G.; Neukirch, L.P.; Usui, Y. Geodynamo, Solar Wind, and Magnetopause 3.4 to 3.45 Billion Years Ago. *Science* **2010**, *327*, 1238–1240. [CrossRef] [PubMed]
75. Nagy, L.; Williams, W.; Muxworthy, A.R.; Fabian, K.; Almeida, T.P.; Conbhuí, P.Ó.; Shcherbakov, V.P. Stability of equidimensional pseudo–single-domain magnetite over billion-year timescales. *Proc. Natl. Acad. Sci. USA* **2017**, *114*, 10356–10360. [CrossRef] [PubMed]
76. Donardelli Bellon, U.; Williams, W.; Trindade, R.I.F.; Diaz, A.; Galante, D. Coupling nanoscopic tomography and micromagnetic modelling to assess the stability of geomagnetic recorders. *Commun. Earth Environ.* **2024**, *5*, 563. [CrossRef]
77. Gergov, H.; Muxworthy, A.R.; Williams, W.; Cowan, A.C. Magnetic Recording Fidelity of Basalts Through 3D Nanotomography. *Geochem. Geophys. Geosyst.* **2025**, *26*, e2024GC011776. [CrossRef]
78. Suk, D.; Peacor, D.R.; van der Voo, R. Replacement of pyrite framboids by magnetite in limestone and implications for palaeomagnetism. *Nature* **1990**, *345*, 611–613. [CrossRef]

79. Enkin, R.J.; Yang, Z.; Chen, Y.; Courtillot, V. Paleomagnetic constraints on the geodynamic history of the major blocks of China from the Permian to the present. *J. Geophys. Res.-Solid Earth* **1992**, *97*, 13953–13989. [CrossRef]
80. Zhao, X.; Coe, R.S.; Gilder, S.A.; Frost, G.M. Palaeomagnetic constraints on the palaeogeography of China: Implications for Gondwanaland. *Aust. J. Earth Sci.* **1996**, *43*, 643–672. [CrossRef]
81. Sun, Z.; Yang, Z.; Yang, T.; Pei, J.; Yu, Q. New Late Cretaceous and Paleogene paleomagnetic results from South China and their geodynamic implications. *J. Geophys. Res.-Solid Earth* **2006**, *111*, B3. [CrossRef]
82. Huang, B.; Zhou, Y.; Zhu, R. Discussions on Phanerozoic evolution and formation of continental China, based on paleomagnetic studies. *Earth Sci. Front.* **2008**, *15*, 348–359. (In Chinese with English abstract)
83. Lin, J. The apparent polar wander path for the South China Block and its geological significance. *Sci. Geol. Sin.* **1987**, *22*, 306–315. (In Chinese with English abstract)
84. Lin, J.; Fuller, M.; Zhang, W. Preliminary Phanerozoic polar wander paths for the North and South China blocks. *Nature* **1985**, *313*, 444–449. [CrossRef]
85. Cheng, G.; Sun, Y.; Li, S. China paleomagnetic data list for Cenozoic. *Seismol. Geol.* **1991**, *13*, 184–186. (In Chinese)
86. Enkin, R.J.; Courtillot, V.; Xing, L.; Zhang, Z.; Zhuang, Z.; Zhang, J. The stationary Cretaceous paleomagnetic pole of Sichuan (South China Block). *Tectonics* **1991**, *10*, 547–559. [CrossRef]
87. Huang, K.; Opdyke, N.D. Paleomagnetism of Cretaceous to lower Tertiary rocks from southwestern Sichuan: A revisit. *Earth Planet. Sci. Lett.* **1992**, *112*, 29–40. [CrossRef]
88. Gilder, S.A.; Coe, R.S.; Wu, H.R.; Kuang, G.D.; Zhao, X.X.; Wu, Q.; Tang, X.Z. Cretaceous and Tertiary paleomagnetic results from Southeast China and their tectonic implications. *Earth Planet. Sci. Lett.* **1993**, *117*, 637–652. [CrossRef]
89. Zhao, X.; Coe, R.; Zhou, Y.; Hu, S.; Wu, H.; Kuang, G.; Dong, Z.; Wang, J. Tertiary paleomagnetism of North and South China and a reappraisal of late Mesozoic paleomagnetic data from Eurasia: Implications for the Cenozoic tectonic history of Asia. *Tectonophysics* **1994**, *235*, 181–203. [CrossRef]
90. Wu, H.; Zhu, R.; Bai, L.; Guo, B.; Lu, J. Revised apparent polar wander path of the Yangtze Block and its tectonic implications. *Sci. China Ser. D-Earth Sci.* **1998**, *41*, 78–90. [CrossRef]
91. Wu, H.; Zhu, R.; Courtillot, V.; Bai, L.; Xing, J.; Zhao, Y.; Yang, G. Paleomagnetic results of Paleozoic and Mesozoic rocks from Xingshan-Zigui section in Hubei Province, South China. *Sci. China Ser. D-Earth Sci.* **1999**, *42*, 182–194. [CrossRef]
92. Yoshioka, S.Y.; Liu, Y.Y.; Sato, K.; Inokuchi, H.; Su, L.; Zaman, H.; Otofuji, Y. Paleomagnetic evidence for post-Cretaceous internal deformation of the Chuan Dian fragment in the Yangtze Block: A consequence of indentation of India into Asia. *Tectonophysics* **2003**, *376*, 61–74. [CrossRef]
93. Tong, Y.; Sun, Y.; Wu, Z.; Mao, C.; Pei, J.; Yang, Z.; Pu, Z.; Zhao, Y.; Xu, H. Passive crustal clockwise rotational deformation of the Sichuan Basin since the Miocene and its relationship with the tectonic evolution of the fault systems on the eastern edge of the Tibetan Plateau. *GSA Bull.* **2018**, *131*, 175–190. [CrossRef]
94. Yang, Z.; Sun, Z.; Ma, X.; Yin, J.; Otofuji, Y. Palaeomagnetic study of the early Tertiary on both sides of the Red River fault and its geological implications. *Acta Geol. Sin.* **2001**, *75*, 35–44. (In Chinese with English abstract) [CrossRef]
95. Watson, G.S. Large sample theory of the Langevin distribution. *J. Stat. Plan. Inference* **1983**, *8*, 245–256. [CrossRef]
96. Wang, H.H.; Li, J.H.; Sun, W.T.; Li, W.B. Global paleoplate reconstruction and lithofacies palaeogeography of the Silurian. *J. Palaeogeogr.* **2016**, *18*, 185–196. (In Chinese with English abstract)
97. Tauxe, L.; Butler, R.F.; Van der Voo, R.; Banerjee, S.K. *Essentials of Paleomagnetism*; University of California Press: Berkeley, CA, USA, 2010. [CrossRef]
98. Gradstein, F.; Ogg, J.; Van Kranendonk, M. On the Geologic Time Scale 2008. *Newsl. Stratigr.* **2008**, *43*, 5–13. [CrossRef]
99. Gradstein, F.M.; Ogg, J.G.; Schmitz, M.D.; Ogg, G.M. *The Geologic Time Scale 2012*; Elsevier: Amsterdam, The Netherlands, 2012. [CrossRef]
100. Golonka, J.; Porębski, S.J.; Waśkowska, A. Silurian paleogeography in the framework of global plate tectonics. *Palaeogeogr. Palaeoclimatol. Palaeoecol.* **2023**, *622*, 111597. [CrossRef]
101. Metcalfe, I. Palaeozoic-Mesozoic history of SE Asia. *Geol. Soc. Lond. Spec. Publ.* **2011**, *355*, 7–35. [CrossRef]
102. Bai, L.; Zhu, R.; Wu, H.; Guo, B.; Lu, J. New Cambrian paleomagnetic pole for Yangtze Block. *Sci. China Ser. D-Earth Sci.* **1998**, *41*, 66–71. [CrossRef]
103. Torsvik, T.H.; Van der Voo, R.; Preeden, U.; Mac Niocaill, C.; Steinberger, B.; Doubrovine, P.V.; van Hinsbergen, D.J.J.; Domeier, M.; Gaina, C.; Tohver, E.; et al. Phanerozoic polar wander, palaeogeography and dynamics. *Earth-Sci. Rev.* **2012**, *114*, 325–368. [CrossRef]
104. Golonka, J. Late Devonian paleogeography in the framework of global plate tectonics. *Glob. Planet. Change* **2020**, *186*, 103129. [CrossRef]
105. Shi, X.; Hou, Y.; Shuai, K. Late Paleozoic deep-water stratigraphic succession in central Youjiang basin: Constraints on basin evolution. *Geosci. Front.* **2006**, *13*, 153–170. (In Chinese with English abstract)

106. Xin, Y.; Li, J.; Ratschbacher, L.; Zhao, G.; Zhang, Y.; Dong, S.; Xia, X.; Yu, Y. Early Devonian (415–400 Ma) A-type granitoids and diabases in the Wuyishan, eastern Cathaysia: A signal of crustal extension coeval with the separation of South China from Gondwana. *GSA Bull.* **2020**, *132*, 2295–2317. [CrossRef]
107. Choong, C.M.; Pubellier, M.; Sautter, B.; Gebretsadik, H. Records of the oceanic propagator closure at the southern splay of the Palaeo-Tethys. *Geol. J.* **2022**, *57*, 3881–3915. [CrossRef]

Disclaimer/Publisher's Note: The statements, opinions and data contained in all publications are solely those of the individual author(s) and contributor(s) and not of MDPI and/or the editor(s). MDPI and/or the editor(s) disclaim responsibility for any injury to people or property resulting from any ideas, methods, instructions or products referred to in the content.